Contribution of HONO to the atmospheric oxidation capacity in an industrial zone in the Yangtze River Delta region of China

Jun Zheng[1*], Xiaowen Shi[1], Yan Ma[1,2], Xinrong Ren[3,4,5], Halim Jabbour[1], Yiwei Diao[1,6], Weiwei Wang[6], Yifeng Ge[1], Yuchan Zhang[1], and Wenhui Zhu[1]

[1]Collaborative Innovation Center of Atmospheric Environment and Equipment Technology, Nanjing University of Information Science & Technology, Nanjing 210044, China

[2]NUIST Reading Academy, Nanjing University of Information Science & Technology, Nanjing 210044, China

[3]Air Resources Laboratory, National Oceanic and Atmospheric Administration, College Park, Maryland, USA

[4]Department of Atmospheric and Oceanic Science, University of Maryland, College Park, Maryland, USA

[5]Cooperative Institute for Satellite Earth System Studies, University of Maryland, College Park, Maryland, USA

[6]Key Laboratory for Aerosol-Cloud-Precipitation of China Meteorological Administration, Department of Atmospheric Physics, Nanjing University of Information Science and Technology, Nanjing 210044, China

Correspondence to: Dr. Jun Zheng (zheng.jun@nuist.edu.cn)

Address: School of Environmental Science and Engineering, Nanjing University of Information Science & Technology, Nanjing 210044, China

Tel.: +86-18251919852

Fax: +86-25-58731090

Key points:

- High levels of HONO, with an average of 1.32 ± 0.92 ppbv, were observed near one of the largest industrial zones in the YRD region of China.
- HONO photolysis and alkene ozonolyses contributed the most of OH production and hence the atmospheric oxidation capacity.
- High loading of $PM_{2.5}$ provided additional reaction surfaces for HONO formation.
- Heterogeneous formation mechanisms were the most important daytime HONO sources and were further enhanced by sunlight.

Abstract

A suite of instruments were deployed to simultaneously measure nitrous acid (HONO), nitrogen oxides (NO_x = NO + NO_2), carbon monoxide (CO), ozone (O_3), volatile organic compounds (VOCs, including formaldehyde (HCHO)) and meteorological parameters near a typical industrial zone in Nanjing of the Yangtze River Delta region, China from 1 to 31 December 2015. High levels of HONO were detected using a wet chemistry-based method. HONO ranged from 0.03-7.04 ppbv with an average of 1.32 ± 0.92 ppbv. Elevated daytime HONO was frequently observed with a minimum of several hundreds of pptv on average, which cannot be explained by the homogeneous OH + NO reaction (P_{OH+NO}) and primary emission ($P_{emission}$), especially during periods with high loadings of particulate matters ($PM_{2.5}$). The HONO chemistry and its impact on atmospheric oxidation capacity in the study area were further investigated using a MCM-box model. The results show that during the campaign perid the average hydroxyl radical (OH) production rate was dominated by the photolysis of HONO (7.13×10^6 molecules cm^{-3} s^{-1}), followed by ozonolysis of alkenes (3.94×10^6 molecules cm^{-3} s^{-1}), photolysis of O_3 (2.46×10^6 molecules cm^{-3} s^{-1}) and photolysis of HCHO (1.60×10^6 molecules cm^{-3} s^{-1}), especially within the plumes originated from the industrial zone. Model simulations indicated that heterogeneous chemistry played an important role in HONO

formation. The average nighttime NO_2 to HONO conversion rate was determined to be ~0.8% hr^{-1}. Good correlation between nocturnal HONO/NO_2 and the products of particle surface area density (S/V) and relative humidity (RH), S/V·RH, supports the heterogeneous NO_2/H_2O reaction mechanism. The other HONO source, designated as $P_{unknonwn}$, was about twice as much as P_{OH+NO} on average and displayed a diurnal profile with an evidently photo-enhanced feature, i.e., photosensitized reactions of NO_2 may be an important daytime HONO source. Nevertheless, our results suggest that daytime HONO formation was mostly due to the light-induced conversion of NO_2 on aerosol surfaces but heterogeneous NO_2 reactions on ground surface dominated nocturnal HONO production. Our study indicated that elevated $PM_{2.5}$ level during the haze events can promote NO_2 to HONO conversion by providing more heterogeneous reaction sites and hence increase the atmospheric oxidation capacity, which may further promote the formation of secondary air pollutants.

1 introduction

Nitrous acid (HONO) plays an important role in tropospheric photochemistry because its fast photolysis contributes to the formation of hydroxyl (OH) radical, which is an essential atmospheric oxidant that initiates the oxidation of volatile organic compounds (VOC) to form organic peroxy radicals (RO_2) and hydroperoxyl radical (HO_2). In the present of nitrogen oxides (NO_x = NO + NO_2), these free radicals are the fundamental driving force of photochemical reaction cycles that lead to the formation of ground-level ozone (O_3) and secondary organic aerosols (SOA) (Finlayson-Pitts and Pitts, 1999; Xue et al., 2016). Besides HONO photolysis (R1), the major known OH radical initiation sources include photolysis of O_3 (R2 and R3) and formaldehyde (HCHO) (R4 to R8), and ozonolysis of alkenes (R9) (Finlayson-Pitts and Pitts, 1999). Nevertheless, many field studies have demonstrated that HONO may strongly affect atmospheric oxidation capacity in various environments (Bernard et al., 2016; Elshorbany et al., 2009; Elshorbany et al., 2010; Zhou et al., 2002). In early studies, HONO was believed to be only important as NO_x reservoir during nighttime, when HONO can accumulate in the atmosphere and give

a boost of photochemistry in the following early morning (Platt et al., 1980). However, recent field studies have demonstrated that high concentrations of HONO are often present in the relatively polluted urban areas during the day. Because of high levels of HONO, the photolysis of HONO becomes an important OH source not only in the early morning but also throughout the day and can contribute up to 30-90% of OH radical during daytime (Acker et al., 2006; Hendrick et al., 2014; Kleffmann et al., 2005; Neftel et al., 1996; Spataro et al., 2013; Su et al., 2008; Zhou et al., 2002).

$$HONO + h\nu\ (300\ nm < \lambda < 405\ nm) \rightarrow OH + NO \quad (R1)$$

$$O_3 + h\nu\ (\lambda < 319\ nm) \rightarrow O(^1D) + O_2 \quad (R2)$$

$$O(^1D) + H_2O \rightarrow 2OH \quad (R3)$$

$$HCHO + h\nu\ (\lambda < 330\ nm) \rightarrow H + HCO \quad (R4)$$

$$HCHO + h\nu\ (\lambda < 361\ nm) \rightarrow H_2 + CO \quad (R5)$$

$$H + O_2 \rightarrow HO_2 \quad (R6)$$

$$HCO + O_2 \rightarrow HO_2 + CO \quad (R7)$$

$$HO_2 + NO \rightarrow NO_2 + OH \quad (R8)$$

$$Alkenes + O_3 \rightarrow OH + other\ products \quad (R9)$$

Despite the significance of HONO in daytime photochemistry, the sources and formation mechanisms of HONO, especially during daytime, are still uncertain. Traditionally, the reaction between NO and OH was thought to be the most important homogeneous source for HONO (Perner and Platt, 1979):

$$OH + NO + M \rightarrow HONO \quad (R10)$$

However, reaction R10 alone cannot sustain the high HONO level observed during daytime in many studies, in which the observed HONO levels were often an order of magnitude greater than the modeled HONO with only homogeneous HONO source (R10) included in the model (Ren et al., 2010; Tang et al., 2015). Nevertheless, higher than expected OH observed in several studies (Hofzumahaus et al., 2009) may explain partially observed higher

than model predicted HONO levels. It has been suggested that HONO may be emitted directly by incomplete combustion processes, such as vehicle exhaust (Kirchstetter et al., 1996; Kurtenbach et al., 2001; Liang et al., 2017; Nakashima and Kajii, 2017; Trinh et al., 2017; Xu et al., 2015) and biomass burning (Müller et al., 2016; Neuman et al., 2016; Nie et al., 2015; Rondon and Sanhueza, 1989). However, such strong but sporadic point sources could not account for the widely observed daytime HONO in the polluted areas (Elshorbany et al., 2012; Wang et al., 2017). Recently, many other HONO formation pathways have been proposed. Su et al. (2011) pointed out that HONO can be released from soil nitrite, which was formed through biological nitrification and denitrification processes. Recent studies demonstrated that the pH and organic content of soil could influence the HONO emission rate (Scharko et al., 2017; Sörgel et al., 2015). In addition, vertical profiles of HONO measurements indicated that HONO was very likely originated from the ground surface (Kleffmann et al., 2003; VandenBoer et al., 2013; Wong et al., 2011; Wong et al., 2013). However, the presence of in-situ HONO sources in the air masses aloft cannot be ruled out (Wong et al., 2013; Zhang et al., 2009).

Several heterogeneous processes have been drawn substantial attention and are proposed as the major HONO sources, including: (1) heterogeneous conversion of NO_2 on wet surface (Finlayson-Pitts et al., 2003), which could be an important nocturnal HONO source; (2) NO_2 heterogeneous reaction with fresh soot particles (Ammann et al., 1998; Gerecke et al., 1998; Han et al., 2017a; Monge et al., 2010) and semi-volatile organic compound emitted from diesel exhausts (George et al., 2005; Gutzwiller et al., 2002), which could be an important process because it is 1 to 2 orders of magnitude faster than the typically proposed heterogeneous reaction of $2NO_2 + H_2O$; (3) photosensitized reaction of NO_2 on surfaces of mineral dust (Ndour et al., 2008), humic acid (Han et al., 2017b; Wall and Harris, 2016), and ground surface (i.e., certain reactions such as NO_2 + humic acids on ground surfaces) (Wong et al., 2012), which has been considered as an important daytime HONO source (Lee et al., 2016); (4) photolysis of adsorbed nitric acid (HNO_3) and nitrate (NO_3^-) (Ye et al., 2016; Ye et al., 2017; Zhou et al., 2002; Zhou et al., 2003; Zhou et al., 2011; Ziemba et al., 2010); (5) VOC-mediated conversion of HNO_3 into HONO

(Gall et al., 2016).

Since the first atmospheric HONO measurement by Nash (1974) and the first use of long path differential UV absorption technique (LP-DOAS) to measure atmospheric HONO (Perner and Platt, 1979), various measurement techniques for HONO have been developed, such as spectroscopic techniques, wet chemistry-based techniques, and chemical ionization mass spectrometry (CIMS). Besides DOAS technique, other spectroscopic techniques such as the cavity ring-down spectroscopy (Rairoux et al., 2002), the incoherent broadband cavity-enhanced absorption spectroscopy (IBBCEAS) (Gherman et al., 2008), and the cavity-enhanced absorption spectrometer (CEAS) (Scharko et al., 2017) were applied in the HONO measurements. Wet chemistry techniques have the advantages of higher sensitivity and lower detection limit, including long path absorption photometer (LOPAP) (Heland et al., 2001; Kleffmann et al., 2003; Kleffmann et al., 2005; Kleffmann et al., 2006; Kleffmann and Wiesen, 2008; Vecera and Dasgupta, 1991), AIM-IC analysis system and wet-rotating-denuder (WRD) method (Makkonen et al., 2012). Very recently, CIMS techniques have been developed for fast on-line HONO measurements (Bernard et al., 2016; Pinto et al., 2014; Ren et al., 2010).

Yangtze River Delta (YRD) region is the largest industrial zone in China and is experiencing ever increasing air pollution events, characterized with high ozone (O_3) and fine particulate matters ($PM_{2.5}$) concentrations (Ding et al., 2013). Despite of the great efforts in reducing sulfur dioxide (SO_2) and NO_x emissions from industrial activities, high level of NO_x along with ammonia/amines have been observed near an industrial park (Zheng et al., 2015b). In addition, high levels of HCHO have been frequently observed near industrial zones in China (Ma et al., 2016; Wang et al., 2015b), providing an extra radical source. HONO concentrations calculated using a photostationary state (PSS) approach that included homogeneous sources were found much less HONO than the measured values during daytime (Kleffmann et al., 2005; Michoud et al., 2014). Lee et al. (2016) conducted a detailed analysis of HONO budget and proposed that the missing daytime HONO source was related to NO_2 and sunlight. A four-season measurement campaign was carried out in an urban site of Beijing and the results showed

monthly averaged HONO concentrations between 1.05 and 2.27 ppbv with pronounced seasonal profile (Wang et al., 2017). In a recent study, Nie et al. (2015) revealed the influence of biomass burning on HONO formation at a suburban site of Nanjing and demonstrated that the contribution of heterogeneous conversion of NO_2 to HONO formation. However, so far, no comprehensive study on the oxidizing capability, i.e., the major contributors of OH radicals, has ever been conducted in the industrial zone of YRD region.

In this work, we have performed HONO measurements using a custom-built wet chemistry-based method at an industrial site in December 2015 in Nanjing, China. In addition, HCHO, O_3, photolysis frequencies, and other trace gases and meteorological parameters were also measured. The contributions of HONO along with other OH sources to OH budget were investigated using a box model based on Master Chemical Mechanism (MCM). The mechanisms of possible daytime HONO formation and the consequent impacts on air pollutants formation were explored.

2 Experimental and Model Description

2.1 HONO Measurement

The field measurements were carried out from 1 to 31 December 2015 on the campus of Nanjing University of Information Science and Technology (NUIST) in Nanjing, China. More details about the observation site have been provided in our previous work (Ma et al., 2016; Zheng et al., 2015b). Briefly, the site is located to the west of clusters of steel mills and petrochemical refinery facilities and is about 15 km to the north of the downtown Nanjing. All instruments were placed inside an air-conditioned trailer. In this study, a custom-built wet chemistry-based HONO instrument was utilized for HONO measurements, which was originally developed by Ren et al. (2010). Figure 1 is the schematics of the HONO instrument, consisting of two sample collection glass coils connected

154 successively, a 10-port injection valve (Valco Instruments Co. Inc.), a 1-m long liquid waveguide capillary cell
155 (LWCC, World Precision Instruments), and a mini spectrometer (Ocean optics, USB4000). Two coil samplers in
156 serial were used to measure total signals in the first sampler and the background in the second sampler. The
157 difference between the two samplers is the net HONO signal. The background signal is usually only a few percent
158 of the total signal.

159 To minimize the sampling artifacts, the sampling coils were set up about 3.5 m above the ground (1.5 m above
160 the trailer rooftop) and no inlet was used. Ambient air was pulled through the coils by a vacuum pump at 1 L min^{-1}
161 , which was controlled by a mass flow controller (MKS, model M100B). In the first coil, HONO along with some
162 interfering species in the air sample were separated from the gas phase and transformed into nitrite solution by a
163 1.0 mmol L^{-1} phosphate buffer scrubbing solution. Potential interfering species (e.g., NO_2) would also interact with
164 scrubbing solution in the second coil in a similar way as in the first coil. The nitrite solutions from the two coils
165 were then respectively mixed with sulfanilamide/N-(1-naphthyl) ethylene-diamine (SA/NED) reagents in Teflon
166 derivatization tubing and nitrite was converted via the two reactions (SR1 and SR2, see the SI for details) (Huang
167 et al., 2002). The aqueous sample was injected into the LWCC and the produced azo dye was quantified by its
168 absorption at 560 nm with a mini USB spectrometer. The difference between the absorbance signals of the two
169 coils was treated as the actual HONO signal. The HONO mixing ratio in ambient air was calculated using Eq. (1):

170 $$[\mathrm{HONO}]_{\mathrm{pptv}} = \frac{C_l F_l RT}{F_g P} \times 10^{12} \qquad (1)$$

171 where, C_l is nitrite concentration (mol L^{-1}) in the scrubbing solution, F_l is the liquid flow rate (mL min^{-1}) of the
172 scrubbing solution, F_g is the sampling air flow rate (L min^{-1}), R is the ideal gas constant (8.314 m^3 Pa K^{-1}mol^{-1}),
173 and T and P are the ambient temperature (294 K) and atmospheric pressure (101325 Pa), respectively, under which
174 the mass flow controller (MFC) that was used to control the sample flow rate was calibrated (Ren et al., 2010). The
175 instrument calibration was carried out once every four days by injecting standard sodium nitrite ($NaNO_2$) solution
176 into the instrument right after the sampling coil. According to the calibration curve, HONO mixing ratio in ambient

177 air can be quantified. The detection limit of the HONO instrument was about 3 pptv with a time resolution of 2
178 min. The measurement accuracy was about ±15% at a 95% confidence level (Ren et al., 2010).

179 **2.2 Other measurements**

180 As the observation site was part of a national standard meteorology observatory facility, meteorology
181 parameters, including wind direction, wind speed, ambient temperature, pressure and RH were continuously
182 measured. Trace gases, CO (Thermo Scientific, Model 48i), O_3 (Thermo Scientific, Model 49i), SO_2 (Thermo
183 Scientific, Model 43i) and NO_x (Thermo Scientific, Model 17i) were also measured at the observation site. The
184 Thermo Scientific 17i is designed as an ammonia (NH_3) analyzer. It basically consists of a typical NO_x analyzer
185 and an external high temperature (700°C) NH_3 converter, which is disabled and bypassed in this work. Therefore,
186 it was used as a typical NO_x analyzer. It is well known that a NO-NO_x analyzer with a molybdenum-based converter
187 can convert portion of NO_z (=NO_y-NO_x) to NO, which can then be detected as NO_2 causing an interference in NO_2
188 measurement (Villena et al., 2012). However, an aircraft study conducted in the eastern US in the winter 2015
189 found that within 6 hours of transport time, NO_x account for more than 90% of NO_y in an urban outflow (Salmon
190 et al., 2018). A sensitivity analysis showed that by decreasing the NO_2 level of 10% (an upper limit assuming all
191 NO_z were converted into NO with an efficiency of 100%), the modeled HONO decreased only by 5.3%, indicating
192 that the possible small interference in NO_2 measurement did not impact significantly on the modeled HONO results.
193 The details about the operation and calibrations of these instruments were described in previous work (Zheng et al.,
194 2015b). $PM_{2.5}$ was observed by an online $PM_{2.5}$ measuring instrument (METONE, BAM-1020) with a time
195 resolution of 1 hour. Aerosol surface area density was calculated using data from an WPS (wide particle
196 spectrometer , MSP model 1000XP) with a time resolution of 5 min. HCHO was measured with the DNPH method
197 from 19 to 30 December 2015 and the sampling time was 2 hours during the campaign. Detailed operation
198 procedures about the DNPH method in this study can refer to our previous work (Ma et al., 2016). Photolysis

199 frequencies (J values), including $J(O^1D)$, $J(NO_2)$, J(HONO), $J(H_2O_2)$, J(HCHO), and $J(NO_3)$, were calculated based
200 on measurements by an ultra-fast charged coupled device (CCD) detector spectrometer (Meteorology Consult
201 Gmbh, Germany). The acquisition time for J values was 1 min. Other photolysis frequencies (such as carbonyls
202 with more than two carbons) used in the model were calculated by Eq. (2) (Jenkin et al., 1997):

203 $$J_i = L_i \cos(\chi)\, M_i \exp(-N_i \sec(\chi)) \qquad (2)$$

204 where χ is the solar zenith angle; L_i, M_i, and N_i are photolysis parameters and are taken from (Jenkin et al., 1997),
205 for clear sky conditions. The calculated photolysis frequencies were then scaled by the measured $J(NO_2)$ for
206 cloudiness correction.

207 Volatile organic compounds (VOC) measurements were conducted using a commercial gas chromatograph
208 equipped with a flame ionization detector (GC-FID) (AMA, GC5000). Sixty VOC species including C_2-C_{12}
209 hydrocarbons were detected with a time resolution of 1 hr. Ten of the most reactive alkenes were used in the
210 ozonolysis reaction in the box model simulations. Although the oxygenated VOCs (OVOCs) other than
211 formaldehyde and some other carbonyls (by the DNPH method) were not measured in this study, they were
212 simulated in the box model that was constrained to measured VOCs. Our results indicated that OVOCs only
213 accounted for a small portion of the total VOCs in this industrial area and even contributed much less to the total
214 VOC OH reactivity. Therefore, the limited VOCs detected in this work would not significantly affect the following
215 model simulation results.

216 **2.3 Box Model**

217 To evaluate the effect of HONO on daytime atmospheric oxidation capacity, a chemical box model with the
218 Master Chemical Mechanism (MCMv3.2) (Jenkin et al., 2012) was applied to calculate the concentrations of OH,
219 HO_2 radicals and their production and loss rates using the FACSIMILE software package (UES Software Inc.).
220 Kinetic rate coefficients were taken from the MCM website (http://mcm.leeds.ac.uk/MCM/). In this study, the

model simulation was constrained with hourly averaged measurement results, including HONO, O_3, NO, NO_2, CO, SO_2, HCHO, VOCs, as well as water vapor, temperature, pressure, and photolysis frequencies.

Monte Carlo sensitivity analyses were conducted to assess the model performance. In each Monte Carlo simulation, the input variables of the model, including HONO, O_3, NO, NO_2, CO, SO_2, HCHO, VOCs, reaction rate constants, photolysis frequencies and the planetary boundary layer (PBL) height were independently set to vary within ±10% of the mean value of individual variable with a normal probability distribution.

3 Results and Discussion

3.1 Data Overview

Figure 2 shows the time series of NO, NO_2, O_3, $PM_{2.5}$, HONO, HCHO, J(HONO), and meteorological parameters, including wind direction, wind speed, temperature, and RH. During the entire campaign period, the wind speed ranged from 0.1 to 8.1 m s^{-1} with an average of 1.7 m s^{-1}. The temperature varied between -4.1 and 16.1 °C with an average of 6.1 °C; RH varied from 17 to 96 % with an average of 68 %.

During the entire measurement period, the HONO mixing ratios ranged from 0.03 to 7.04 ppbv with a mean value of 1.32 ± 0.92 ppbv. Table 1 lists recent HONO observations conducted in China. Our result was comparable to HONO observed in Xinken (Su et al., 2008) and Beijing (Spataro et al., 2013; Wang et al., 2017) but higher than Xianghe, Beijing (Hendrick et al., 2014), Jinan (Wang et al., 2015a), Hong Kong (Xu et al., 2015) and Shanghai (Wang et al., 2013). Clearly, the general trend of HONO was closely following that of NO_2, which is the dominant precursor of HONO. More markedly, building up of HONO frequently proceeded the accumulations of $PM_{2.5}$, e.g., on the 7th and from the 21st - 22nd of December 2015, indicating that HONO may promote the formation of secondary aerosol by contributing to OH production, which will be further analyzed in details in the following

242 sections. The campaign averaged diurnal variations of HONO, NO_2, HONO/NO_2 ratio and aerosol S/V are showed
243 in Fig. 3. HONO started to accumulate after sunset and reached its daily averaged maxima of ~2.0 ppbv at 08:00
244 local time (LT). Later the day, the HONO mixing ratio decreased rapidly due to its fast photolysis and increase of
245 the PBL height. Evidently, daytime HONO was sustained at a relatively high level. The daily averaged minimum
246 of ~0.6 ppbv was observed around 16:00 LT. The mixing ratio of NO_2 varied from 9.5 to 48.7 ppbv with an average
247 of 23.9 ± 7.5 ppbv and a daily averaged maximum of 27.7 ± 8.8 ppbv. NO, O_3 and $PM_{2.5}$ mixing ratios were in the
248 range of 2.7 to 124.9 ppbv, 3 to 39 ppbv and 15 to 345 μg m^{-3}, respectively. Meanwhile, the HONO-to-NO_2 ratios
249 ranged from 0.02 to 0.07, with an average of 0.05 ± 0.03.

250 **3.2 OH Simulation**

251 Although atmosphere oxidation capacity is determined by the levels of all major oxidants in the atmosphere
252 (e.g., OH, O_3, and NO_3), OH radical is the primary oxidant in the atmosphere and series of reactions initiated by
253 OH radical can lead to the formation of other major secondary oxidants, such as O_3 and NO_3. Fully understanding
254 the budget of OH radical especially the sources of OH radical is of paramount importance for the purpose of
255 controlling the atmosphere oxidation capacity and hence to establish effective air pollution mitigation strategies.
256 *In-situ* measurement of OH radical is often limited by the availability of suitable measurement techniques,
257 which are often suffered from large amount of unresolved uncertainties (Tanner and Eisele, 1995) and the
258 observation often disagree with the modeling results to a large extent. Nevertheless, theoretically some critical
259 parameters to govern the OH radical budget in the atmosphere are difficult to measure directly, such as the
260 formation rates of OH. Accordingly, a box model is often utilized to simulate these highly reactive species to
261 investigate their photochemistry.
262 In order to assess the relative contributions of potential OH sources in this study, we have utilized a box model
263 based on the Master Chemical Mechanism (MCMv3.2) (Jenkin et al., 2012) to simulate the OH concentration and

the OH formation rates from various sources. The model simulation was constrained by the measurement results, including HONO, O_3, NO, NO_2, CO, SO_2, VOCs, as well as water vapor, temperature, pressure, and photolysis frequencies. Since HCHO measurement was only available from 19 to 30 December, simulated HCHO was used for the entire campaign period. We found that the ratio between simulated to measured HCHO was 1.4 with a correlation coefficient of R = 0.77. Therefore, we applied a factor of 1.4 to the simulated HCHO in the model to better represent the HCHO concentration in the atmosphere.

The simulated OH time series during the campaign period is shown in Fig. 4. Because the simulation is constrained by the observations, only within periods when all data are available simulation were conducted. Simulated OH concentration was in the range of 1.06×10^6 to 5.26×10^6 molecules cm^{-3}, similar to the concentration observed in London (Emmerson et al., 2007), but lower than that measured in New York City (3×10^6 to 3.3×10^7) (Ren et al., 2003) and Guangzhou (1.5×10^7 to 2.6×10^7) (Lu et al., 2012).

It should be noted that the absolute values of the simulated OH may differ from the actual ambient concentration. However, the general trend of OH evidently followed the solar radiation intensity, indicating its photochemical production origin. Clearly, the diurnal variation of OH profile is more complicated than that of photolysis rates becasue OH production can be affected not only by photochemical processes, but also by both primary emissions (e.g., HONO and HCHO) and other non-photochemical related heterogeneous processes, such as HONO production on various surfaces and ozonolysis of alkenes. These processes will be further discussed in the following sections.

3.3 OH Formation Rates

$$P_{OH}(HONO)_{net} = J(HONO)[HONO] - k_{OH+NO}[NO][OH] \quad (3)$$

$$P_{OH}(O_3) = 2\,J(O^1D)[O_3]\emptyset_{OH} \quad (4)$$

$$P_{OH}(HCHO) = 2J(HCHO)[HCHO] \quad (5)$$

$$P_{OH}(H_2O_2) = 2J(H_2O_2)[H_2O_2] \quad (6)$$

$$P_{OH}(O_3 + alkenes) = \sum k_{alkene(i)+O3}[alkene(i)][OH]Y_{OH\_i} \quad (7)$$

Previous field studies have demonstrated that HONO photolysis can contribute substantially to the OH production during daytime (Elshorbany et al., 2009; Hendrick et al., 2014; Kleffmann et al., 2005; Su et al., 2008). In this study, we evaluated the OH formation rates from the photolysis of HONO (Eq. 3), ozone (Eq. 4), formaldehyde (Eq. 5) and hydrogen peroxide (H_2O_2) (Eq. 6), as well as ozonolysis of alkenes (Eq. 7). The second term in Eq. 3 is to account for the loss of OH due to the HONO formation from OH + NO, where the OH concentration was simulated using the box model, so that the net OH formation from the photolysis of HONO is considered. J values are the photolysis frequencies of the corresponding species and ϕ_{OH} is the fraction of $O(^1D)$ reacts with H_2O instead of being quenched by nitrogen (N_2) or oxygen (O_2). The OH production by the photolysis of formaldehyde was calculated assuming that HO_2 formed from reaction R4 was immediately converted into OH by reaction R8 due to high NO levels in this polluted environment. In Eq. 7, Y_{OH_i} is the yield of OH from gas-phase reaction of O_3 and alkene(i) and $k_{a\mathrm{lkene(i)}+O_3}$ is the reaction rate constant for the reaction of O_3 with alkene(i). The rate constants of the ozonolysis reactions and the corresponding OH yields used in this work are listed in Table 2. Since H_2O_2 was not measured during this campaign, H_2O_2 was estimated from literature values, i.e., 0.5 to 5 ppbv (Guo et al., 2014; Hua et al., 2008; Ren et al., 2009) and a constant of 3 ppbv H_2O_2 was used in this work.

The calculated campaign averaged OH production rates from the photolysis of HONO, O_3, HCHO and H_2O_2 along with ozonolysis of alkenes were 7.13×10^6, 2.46×10^6, 1.60×10^6, 2.39×10^5 and 3.94×10^6 molecules cm^{-3} s^{-1}, respectively, which were comparable with the literature values (Alicke et al., 2002; Chan et al., 2017; Su et al., 2008). As shown in Fig. 5, the contribution of HONO photolysis to OH production during 7:00-16:00 local time varied from 23.6 to 63.3% with a mean value of 44.8%. The ozonolysis of ten highly reactive alkenes (listed in Table 2) by ozone was the second largest contributor to OH radical and the contribution varied from 16.1 to 60.9% with a mean of 30.3%. The contribution of ozone photolysis was in the range of 1.3 to 24.7% with a mean of 14.9%.

309 The contribution of HCHO photolysis varied between 0.9 and 12.5% with a mean of 8.1%, and the contribution of
310 H_2O_2 photolysis was negligible with an average contribution of 1.9%. The contributions from different OH sources
311 in this study was similar to those found in two wintertime studies. In a study conducted in New York City in winter
312 2004, it was found that 48% of the net HO_x production was from the HONO photolysis, 36% from the ozonolysis
313 of alkenes, only 6% from the HCHO photolysis, and 1% from the O_3 photolysis (Ren et al., 2006). In another study
314 conducted in London in winter 2000, 62% of the OH production was found from the ozonolysis of alkenes, 35%
315 from the HONO photolysis, only 6% from the HCHO photolysis, and <1% from the O_3 photolysis (Heard et al.,
316 2004).

317 The striking features of the Fig. 5 is that HONO photolysis and ozonolysis of alkenes contributed more than
318 70% of the OH production rate on average. In the early morning, HONO photolysis was the dominant source of
319 OH and may boost the photochemistry right after sunrise. As O_3 accumulated, alkene ozonolysis and O_3 photolysis
320 became more and more important. The higher percentage of the HONO photolysis in this study is most likely
321 because of the higher concentrations of HONO observed in the study area and its sources will be further investigated
322 in the following sections.

323 **3.4 Industrial Plumes**

324 Industrial emissions are responsible for a large portion of the haze formation in China. With the
325 implementations of more and more strict mitigation strategies, primary emissions have been reduced substantially
326 in China. However, the observation site was located just ~5 km from the Nanjing industry park, one of the largest
327 industrial zones in the YRD region, which is populated with various heavy industry facilities, including steel mills,
328 power generation stations, and petrochemical refineries. Despite the great effort to reduce primary industrial
329 emissions from these facilities, industrial plumes have often been detected at the site, carrying fair amounts of NH_3,
330 NO_x, SO_2, and VOCs (Ma et al., 2016; Zheng et al., 2015a). To investigate the effects of industrial emissions on

local and regional air quality and particularly the role of HONO on the transformation of primary emissions into secondary air pollutants, we have paid special attention into the air masses originated from the industrial zone. Figure 6 depicts the contribution fractions of OH production rates from HONO photolysis, alkene ozonolysis, O_3 photolysis, HCHO photolysis, and H_2O_2 photolysis during two industrial plume events. The wind rose plots in Fig. 6 indicate that the origins of these air masses were all from the nearby industry zone. Unlike that depicted in Fig. 5, during the two industry pollution events HONO photolysis along with ozonolysis of alkenes dominated the OH production throughout the day. This was most likely due to the high concentrations of NO_x and VOC within the industrial plumes. More interestingly, the average $PM_{2.5}$ concentrations during the two events were 139 and 239 μg m^{-3}, respectively. Evidently, HONO photolysis and ozonolysis may even play a more important role in OH production during severe haze events. Although ambient OH concentrations during these events may not be high (see Fig. 4a), the high levels of HONO can boost active photochemical oxidation and thus promote the formation of other secondary air pollutants.

3.5 HONO Sources

3.5.1 Primary HONO Emissions

Previous studies have demonstrated that HONO can be emitted directly from vehicle exhaust (Kirchstetter et al., 1996; Kurtenbach et al., 2001). However, the NO/NO_x ratio measured in this work was relatively low, with an average of 0.25±0.06, much less than that of freshly emitted exhausts (> 0.9) obtained from tunnel experiments (Kurtenbach et al., 2001), indicating that the air masses sampled in this work had been considerably aged and mixed with other air masses, and hence primary HONO from direct emissions (if there was any) had been diluted substantially (less than a few per cents) before reaching the observation site. In addition, our sampling site is located nearby the industrial zone, and the high concentration of NO_x was mainly originated from the industrial activities, so the influence of traffic source on HONO was expected to be small. To further evaluate the potential impact of

primary emissions on HONO concentration, we have incorporated the contribution of primary HONO emissions into the MCM box model. The HONO emission ratios, i.e., HONO/NO_x, was taken as 0.3% (Kirchstetter et al., 1996), representing a gasoline-fueled vehicle fleet, which was very typically encountered in the study area. On average, the primary emissions from vehicle exhaust can only account for 11% of the total HONO concentration, indicating secondary mechanisms still dominated HONO level in the study area, which will be further analyzed in the following sections.

3.5.2 HONO Conversion Rate

In addition to primary emission, heterogeneous reactions of NO_2 on surfaces are believed to be the major formation pathways of nocturnal HONO. In order to discuss the influence of secondary mechanisms on HONO, the observed HONO was corrected by removing the portion of primary emission ($HONO_{emis}$) and was denoted as $HONO_{corr}$ (= HONO - $HONO_{emis}$).

The HONO conversion rate k(het) (hr^{-1}) is an important parameter to compare HONO formation under various NO_2 levels (Xu et al., 2015). In this work, we calculate the HONO conversion rate using the Eq. (8) (Alicke et al., 2003):

$$k(het) = \frac{[HONO_{corr}]_{t_2} - [HONO_{corr}]_{t_1}}{(t_2 - t_1)[NO_2]} \quad (8)$$

where $[HONO_{corr}]_{t1}$ and $[HONO_{corr}]_{t2}$ are the corrected HONO concentrations at two different times, t_1 and t_2, respectively, $[NO_2]$ is the average NO_2 concentration between time t_1 and t_2. The time periods used to calculate HONO/NO_2 conversion ratio were selected when both HONO and NO_2 increased monotonically with a correlation coefficient higher than 0.8. Note Eq. (8) is a simplified demonstration to calculate the reaction rate coefficient of the heterogeneous conversion from NO_2 to HONO at night, which can be dependent on different pollution levels. In this study, the averaged k(het) was determined to be ~0.8% hr^{-1}, which was comparable to the results in the urban sites of Xi'an (0.91% hr^{-1}) (Huang et al., 2017) and Shanghai (0.7% hr^{-1}), China (Wang et al., 2013), but much less

than some other observations, such as Back Garden, Guangdong, China (2.4% hr^{-1}) (Li et al., 2012), Xinken, Guangdong, China (1.6% hr^{-1}) (Li et al., 2012) and Rossfeld, Rhine Valley, France (2.2% hr^{-1}) (Acker and Möller, 2007). Nevertheless, the high level of NO_x observed in this work may still lead to high level of HONO through various mechanisms.

3.5.3 Heterogeneous Conversion of NO_2

Previous studies have suggested that heterogeneous conversion of NO_2 on wet surfaces could be an important nocturnal HONO source (Finlayson-Pitts et al., 2003; Wang et al., 2017). However, it appears that the proposed reaction mechanism ($2NO_2 + H_2O$) was limited by the uptake of NO_2 on the wet surfaces (on the order of 10^{-6}) and thus was too slow to account for the observed NO_2 to HONO conversion ratio (Kleffmann et al., 1998). Instead, the reaction between NO_2 and adsorbed semi-volatile organic compounds on soot or aerosol surfaces has been suggested to be one to two orders of magnitudes faster than the aforementioned reaction (George et al., 2005; Gutzwiller et al., 2002) even though the actual reaction mechanism is still under active research. It also should be noted that during nighttime as ambient temperature decreased, the PBL height also decreased, causing the ground surface to air volume ratio to increase, which may also contribute to higher NO_2 to HONO conversion efficiency (Stutz et al., 2004). However, as shown in Fig. 7, $HONO_{corr}/NO_2$ correlated with S/V to some extent and the correlation increased with the product of RH and S/V. Therefore, even though the contribution of HONO formation on the ground surface was present, the aerosol surface was certainly involved in the HONO formation process. The impact of RH on the heterogeneous formation of HONO was further investigated. Figure 8 shows the relationship between $HONO_{corr}/NO_2$ ratio and RH at night. The linearity of the bin points clearly displays the linear correlations between HONO conversion ratio and RH. Following the method introduced by Stutz et al. (2004), we plotted the top-5 values of $HONO_{corr}/NO_2$ ratio (representing steady state conditions) in each 10% RH interval. The conversion efficiency of NO_2 to HONO correlates very well with RH (R=0.98), strongly indicating the dependence of HONO

formation on RH. Similar phenomenon was also observed at an urban site (Qin et al., 2009) and a rural site (Li et al., 2012) in Guangzhou, China.

3.5.4 Daytime HONO Budget

High concentrations of daytime HONO were frequently observed during the campaign period especially within industrial plumes. If we assume HONO was in photostationary state involving only gas-phase homogeneous HONO production and photolysis loss, the calculated daytime HONO concentration would be 8.1×10^9 molecules cm^{-3}, only 24.5% of the observed mean HONO concentration during daytime. Since the gas phase reaction between OH and NO (i.e., P_{OH+NO}) and primary emission ($P_{emission}$) were unable to explain the observed high HONO concentrations, daytime HONO budget was further examined in details. Here we designate the unexplained HONO source as $P_{unknown}$. The temporal variation of measured HONO concentration can be expressed by the following equation (Wang et al., 2017):

$$\frac{d[HONO]}{dt} = (P_{OH+NO} + P_{emissions} + P_{unknown}) - (L_{OH+HONO} + L_{photolysis} + L_{deposition}) \quad (9)$$

Thus, $P_{unknown}$ can be calculated as:

$$\begin{aligned} P_{unknown} &= \frac{d[HONO]}{dt} + L_{OH+HONO} + L_{photolysis} + L_{deposition} - P_{OH+NO} - P_{emission} \\ &= \frac{d[HONO]}{dt} + k_{OH+HONO}[OH][HONO] + J_{HONO}[HONO] + \frac{v_{HONO}}{H}[HONO] \\ &\quad -k_{OH+NO}[OH][NO] - \frac{0.003\Delta NOx}{\Delta t} \end{aligned} \quad (10)$$

where d[HONO]/dt represents the variation of observed HONO concentrations; $L_{photolysis}$ represents the loss rate of HONO by photolysis and J_{HONO} is the measured photolysis frequency of HONO; P_{NO+OH} and $L_{OH+HONO}$ are the gas-phase formation and loss rates of HONO, respectively; k_{OH+NO} and $k_{OH+HONO}$ are the corresponding reaction rate constants; $L_{deposition}$ is the dry deposition rate of HONO; v_{HONO} represents deposition velocity of HONO and H is the mixing height; the last term represents direct emissions of HONO. For v_{HONO}, a value of 0.48 cm s^{-1} was

adopted (Lee et al., 2016) and the observed mixing height varied from 73 m to 600 m diurnally. A sensitivity analysis with and without the HONO deposition shows that the modeled HONO concentration with HONO deposition loss is 3.5% lower than that without HONO deposition during daytime, indicating that the dry deposition of HONO plays a minor role in HONO losses. The impact of HONO direct emissions was relatively small at daytime. Daytime OH concentration was not measured in this work but was simulated by the MCM box model.

Figure 9 shows the average diurnal variation of each individual term in Eq. (10). Compared with $L_{photolysis}$, the gas-phase reaction between OH and HONO and HONO dry deposition contributed very little to the HONO sink during daytime. However, P_{OH+NO} and $P_{unknown}$ both contributed significantly to the HONO production and displayed a completely distinct diurnal pattern. Homogeneous reaction between OH and NO reached a maximum of 1.04 ppbv hr^{-1} in the early morning (09:00 LT) due to high concentrations of NO in the morning. The unknown source reached a maximum of 1.22 ppbv hr^{-1} around noontime with an average of 0.73 ppbv hr^{-1}, which was about twice as much as averaged P_{OH+NO}. The diurnal profile of $P_{unknown}$ showed a strong photo-enhanced feature, which is consistent with that observed by Michoud et al. (2014) in wintertime Europe.

3.5.5 Photo-Enhanced Conversion of NO_2

The nature of the unknown source was explored by correlation analyses between $P_{unknown}$ and other HONO production related parameters (see Table 3). $P_{unknown}$ does not correlate well with RH, NO_2, S/V, and J_{NO2} with the correlation coefficients (R) of 0.27, 0.31, 0.33, and 0.31 respectively. The correlation increased only slightly when heterogeneous conversion of NO_2 (NO_2·RH, R = 0.40) was taken into consideration. It appeared that the unknown HONO sources cannot be well explained by the heterogeneous reactions on wet surfaces alone. Previous studies have suggested that light intensity could be an important parameter influencing the heterogeneous conversion of NO_2 to HONO (Han et al., 2017b; Lee et al., 2016). The photo-enhanced HONO source during the daytime has also been identified in different environments ranging from remote (Villena et al., 2011; Zhou et al., 2002) to urban

conditions (Lee et al., 2016). When photo-enhancement was also considered (J_{NO2}·NO_2·RH, R = 0.70), a significantly better correlation was achieved (Table 3). This suggests that the photosensitized reaction of NO_2 on wet surfaces may be an important source of HONO during daytime. Thus, the improvement in the correlation between HONO and other parameters indicates that photochemistry might indeed play an important role in daytime HONO formation (George et al., 2005; Stemmler et al., 2006). Since the correlation coefficient between P_{unknow} and J_{NO2}·NO_2·RH is comparable with the value between P_{unknow} and J_{NO2}·NO_2·S/V·RH (R =0.70), either ground or aerosol surfaces can be the dominant reaction site for photosensitized conversion of NO_2.

Since aerosol chemical composition was not measured in this work, we cannot demonstrate any possible direct connection between aerosol composition and the photo-enhanced HONO formation on aerosol surfaces. Nevertheless, the actual mechanism underlying the photo-enhanced HONO formation on aerosol surface needs further investigation. It has been found that photo-sensitized NO_2 conversion rate coefficient on different surfaces can vary substantially (Han et al., 2017a; Stemmler et al., 2006). Furthermore, studies have shown that this type of surface reaction is not catalytic in nature and the surface reaction rate may vary with the availability and aging state of the surface reaction sites (Stemmler et al., 2006). Therefore, aerosol chemical composition alone may not be sufficient to reveal the actual HONO formation processes.

3.5.6 Model Simulation of HONO

The relative contributions of potential HONO sources were assessed by a box model based on the Master Chemical Mechanism (MCMv3.2) (Jenkin et al., 2012). In addition to the homogeneous reaction of NO with OH, four sources of HONO were included, i.e., heterogeneous HONO formation from NO_2 reaction on aerosol surface and ground surface and light-induced conversion of NO_2 on aerosols and ground surface. Dry deposition of HONO was also considered and a deposition velocity of 0.48 cm s^{-1} was used here (Lee et al., 2016).

Most laboratory studies suggest that the heterogeneous reaction on surface leading to HONO is proportional

to the first order of NO_2 (Finlayson-Pitts and Pitts, 1999), therefore the HONO formation can be represented by the following reactions (Li et al., 2010):

$$NO_2 \xrightarrow{k_a} HONO, \quad (11)$$

$$NO_2 \xrightarrow{k_g} HONO, \quad (12)$$

where k_a and k_g are the first-order rate constants for aerosol and ground surface reactions, respectively. For the heterogeneous reaction on aerosols, the first order rate constant was estimated as:

$$k_a = \frac{\gamma_{NO2,aerosol}\bar{v}(S/V)}{4} \quad (13)$$

where $\bar{v}$ is the root mean square (RMS) velocity of NO_2, S/V is the aerosol surface area-to-volume ratio and $\gamma_{NO2,aerosol}$ is the reactive uptake coefficient on the aerosol surface, with a value of 1×10^{-6} under dark conditions (Aumont et al., 2003; Li et al., 2010). Under sunlight, however, significant enhancement of NO_2 conversion to HONO has been found for various types of aerosol surfaces, such as humic acid and similar organic materials (Stemmler et al., 2007), soot (Monge et al., 2010), and mineral dusts (Ndour et al., 2008). To account for the photoenhancement, a higher value of uptake coefficient (2×10^{-5}) was used for solar radiation less than 400 W m^{-2} and an uptake coefficient scaled by (light intensity)/400 for solar radiation larger than 400 W m^{-2} as suggested by Li et al. (2010). Accordingly, in this work the photoenhanced uptake coefficient was taken as 2×10^{-5} around the morning hours (~9 AM) and was scaled by the measured photolysis rate of NO_2, i.e., $(JNO_2)/ 2\times10^{-3}$ for J_{NO2} higher than 2×10^{-3} (the value of J_{NO2} at ~9 AM).

$$k_g = \frac{V_{d,NO2}}{2H} \quad (14)$$

$$V_{d,NO2} = \frac{\gamma_{NO2,ground}\bar{v}}{4.2} \quad (15)$$

Equation (14) was used to denote the heterogeneous reactions on the ground surfaces, where $V_{d,NO2}$ represents deposition velocity of NO_2; H is the PBL height; and $\gamma_{NO2,ground}$ is the reactive uptake coefficient on the ground. Here we assume an NO_2 reactive uptake coefficient of 1×10^{-5} (Trick, 2004) in the dark on ground surfaces with a yield of 50% and increase it to 2×10^{-5} in the daytime, given that the photosensitized reactivity of NO_2 on the ground

surface is the same as on the aerosol surface. The observed boundary layer height varied from 73 m to 600 m diurnally. The same scale factor ($(JNO_2)/ 2\times10^{-3}$) was also applied to the daytime ground surface reactions.

Figure 10a shows the averaged diurnal profiles of the measured HONO concentration and the simulated HONO concentrations from different sources. In general, the box model can capture the observed HONO trend with very similar magnitude of concentration, with a modeled-to-observed HONO ratio of 1.26 during the day and 1.66 at night. In early morning, ground surface appeared to play an important role in HONO heterogeneous production while the PBL was still relatively shallow. However, after ~9:00, despite of the swift developing of PBL, fine particle loading started increasing substantially (as shown in Fig. 3), indicating strong secondary formation of aerosols. Meanwhile, HONO production on aerosol surfaces also increased moderately. We found that higher daytime values were mostly due to the light-induced conversion of NO_2 on aerosol surfaces in addition to the homogeneous reaction of NO with OH. While at night, heterogeneous HONO production on ground surface dominated nocturnal HONO sources and the nighttime aerosol surfaces only contributed slightly (2.2% and 7.9%, respectively) to the total nighttime HONO,. The box model tended to under-predict HONO during daytime, which also led to a ~1-hr delay in the peaking time of the simulated HONO. The most likely reason for these disagreements is due to the fact that heterogeneous conversion of NO_2 on various surfaces is too complicated to be fully represented by a single scaling parameter in a linear form. Nevertheless, the general agreement between observation and simulation in this work demonstrated that photo-induced NO_2 conversion on aerosol surfaces was the most important HONO source in the study area during daytime.

A Monte Carlo sensitivity analysis was also conducted to assess the model simulation uncertainty of HONO concentration. For each of the 24 hours, 100 independent runs were performed. The Monte Carlo sensitivity analysis show that the model uncertainty of HONO ranged from ±13% to ±38%. The sensitivity analysis reinforced the conclusions that the proposed heterogeneous sources can generally capture the observed HONO trend.

To investigate the interaction between HONO chemistry and secondary aerosol formations within industrial

plumes, we have simulated HONO within the two industrial plume events (see Fig. 6). The results are shown in Fig. 10b. Clearly, HONO was much higher within the industrial plumes comparing to the campaign average (Fig. 10a). In addition, we have performed a model sensitivity study with respect to aerosol surface density by varying S/V from 50% to 200% of the average value. The results showed that the contribution from heterogeneous photosensitized conversion of NO_2 on aerosol surfaces would correspondingly vary from 18% to 40% of the total HONO budget, demonstrating that aerosol surface chemistry played an important role during HONO formation in the study area. Indeed, aerosol surfaces were the most important HONO source during daytime (7:00 -16:00 LT), especially in the afternoon. Within the industrial plumes, aerosol surfaces contributed around 35% of the observed daytime HONO and only about 11% of total HONO was from the ground surfaces. The fact that ground surfaces were less important during daytime than nighttime was most likely due to the much higher daytime PBL, causing substantial dilution of HONO formed on the ground surfaces. Meanwhile, secondary particulate matters were rapidly produced within the PBL, providing additional heterogeneous reaction sites for HONO formation as a strong OH source to further promote atmospheric oxidative capacity. It should be noted that the reactive uptake of NO_2 on various surfaces can be highly variable with the type of surfaces. The value used here ($\sim 2\times10^{-5}$) is toward the lower end of values reported in the literatures, which is likely the reason that the simulated HONO is generally less than the observations within industrial plumes. The heterogeneous NO_2 uptake kinetics and HONO yields of real atmospheric substrates are still under active study and may be different compared to the artificial surfaces studied in the laboratory setting. Nevertheless, enhanced photosensitized conversion of NO_2 on aerosol surfaces is demonstrated here as a major HONO source in the plumes influenced by industrial emissions.

4 Conclusions

Nitrous acid was measured with a custom-built wet-chemistry based HONO analyzer, together with other atmospheric OH precursors (O_3 and HCHO) at a suburb site of Nanjing in December 2015. The mixing ratios of HONO varied from 0.03 ppbv to 7.04 ppbv with an average of 1.32 ± 0.92 ppbv. Daytime HONO was sustained at a relatively high concentration, with a minimum diurnal hourly average of ~0.6 ppbv observed around 16:00 LT. A MCM-box model was used to investigate the HONO chemistry and its impact on atmospheric oxidation capacity in the study area. The results show that the average OH production rates from the photolysis of HONO, ozonolysis of alkenes, photolysis of O_3, HCHO, and H_2O_2 were 7.13×10^6, 3.94×10^6, 2.46×10^6, 1.60×10^6 and 2.39×10^5 molecules cm^{-3} s^{-1} , respectively. The box model results show that the average total OH production rate was 1.54×10^7 molecules cm^{-3} s^{-1} during daytime, on average about 45% from the photolysis of HONO, 30% from ozonolysis of alkenes, 15% from the photolysis of O_3, 8% form the photolysis of HCHO and 2% from the photolysis of H_2O_2.

Elevated daytime HONO evidently played an important role in sustaining the atmospheric oxidative capability in the study area, which cannot be explained by the typical OH+NO homogeneous formation mechanism. The observed similarity between the diurnal profiles of $HONO/NO_2$ ratio and HONO strongly suggests that HONO was most likely originated from NO_2 heterogeneous reactions. In this study, the averaged NO_2 to HONO conversion rate was determined to be ~0.8% hr^{-1} at night. Good correlation between nocturnal $HONO/NO_2$ and the products of S/V·RH supports the heterogeneous NO_2/H_2O reaction mechanism.

To fully assess the HONO chemistry in the study area, an MCM box model was developed to examine HONO budget. In general, the box model can capture the observed HONO trend with a modeled-to-observed HONO ratio of 1.26 during the day and 1.66 at night. The model suggests that higher daytime levels of HONO were mainly produced by the light-induced conversion of NO_2 on aerosol surfaces (28.2%) and ground surfaces (17.8%) (except

early morning). While the heterogeneous HONO production on ground surface dominated nocturnal HONO sources, heterogeneous reactions on various surfaces only contributed a small portion of total HONO at daytime (2.2% on aerosol surface and 7.9% on ground surface). The box model tends to over-predict HONO at night. The most possible reason for these discrepancies is due to the fact that heterogeneous conversion of NO_2 on various surfaces was too complicated to be fully represented by a single scaling parameter in a linear form. Nevertheless, the general agreement between observation and simulation in this work reiterated that photo-induced NO_2 conversion on ground and aerosol surfaces was the most important HONO source in the study area. In the industrial plume case study, it was demonstrated that heterogeneous photosensitized conversion of NO_2 on aerosol surfaces was particularly intensified, when rapid growth of secondary particulate matter was simultaneously observed. Our results indicate that the heterogeneous photosensitized conversion of NO_2 on aerosol surfaces becomes the largest HONO source throughout the daytime, which in turn can enhance OH production, increase the oxidative capacity of atmosphere, and further strengthen the formation of SOA during the daytime in this environment.

Author contributions

JZ, YM, and XR designed the experiments, and XS, HJ, YG, WW, YZ, WZ, and YD carried out the field measurements and data analysis. XS and XR performed the MCM box model simulation. JZ, XS, and YM prepared the manuscript with comments from all coauthors.

Acknowledgements

This work was supported by the National Natural Science Foundation of China (Grant numbers 41730106, 41575122, and 41675126) and the National Key Research and Development Project (Grant number 2017YFC0209501). The data used here are listed in the tables, figures, and the supporting materials.

References

574 Acker, K., Möller, D., Wieprecht, W., Meixner, F. X., Bohn, B., Gilge, S., Plass-Dülmer, C., and Berresheim, H.:
575 Strong daytime production of OH from HNO_2 at a rural mountain site, Geophys. Res. Letts., 33, L02809,
576 10.1029/2005GL024643, 2006.

577 Acker, K., and Möller, D.: Atmospheric variation of nitrous acid at different sites in Europe, Environ. Chem., 4,
578 242-255, https://doi.org/10.1071/EN07023, 2007.

579 Alicke, B., Platt, U., and Stutz, J.: Impact of nitrous acid photolysis on the total hydroxyl radical budget during the
580 Limitation of Oxidant Production/Pianura Padana Produzione di Ozono study in Milan, J. Geophys. Res. Atmos.,
581 107, 8196, 10.1029/2000JD000075, 2002.

582 Alicke, B., Geyer, A., Hofzumahaus, A., Holland, F., Konrad, S., Patz, H. W., Schafer, J., Stutz, J., Volz-Thomas,
583 A., and Platt, U.: OH formation by HONO photolysis during the BERLIOZ experiment, J. Geophys. Res. Atmos.,
584 108, 17, 8247
585 10.1029/2001jd000579, 2003.

586 Ammann, M., Kalberer, M., Jost, D. T., Tobler, L., Rossler, E., Piguet, D., Gaggeler, H. W., and Baltensperger, U.:
587 Heterogeneous production of nitrous acid on soot in polluted air masses, Nature, 395, 157-160, 10.1038/25965,
588 1998.

589 Atkinson, R., and Arey, J.: Atmospheric degradation of volatile organic compounds, Chem. Rev., 103, 4605-4638,
590 10.1021/cr0206420, 2003.

591 Aumont, B., Chervier, F., and Laval, S.: Contribution of HONO sources to the $NO_x/HO_x/O_3$ chemistry in the
592 polluted boundary layer, Atmos. Environ., 37, 487-498, https://doi.org/10.1016/S1352-2310(02)00920-2, 2003.

593 Bernard, F., Cazaunau, M., Grosselin, B., Zhou, B., Zheng, J., Liang, P., Zhang, Y., Ye, X., Daele, V., Mu, Y., Zhang,
594 R., Chen, J., and Mellouki, A.: Measurements of nitrous acid (HONO) in urban area of Shanghai, China, Environ.
595 Sci. Pollut. Res. Int., 23, 5818-5829, 10.1007/s11356-015-5797-4, 2016.

596 Chan, K. L., Wang, S., Liu, C., Zhou, B., Wenig, M. O., and Saiz-Lopez, A.: On the summertime air quality and
597 related photochemical processes in the megacity Shanghai, China, Sci. Total Environ., 580, 974-983,
598 https://doi.org/10.1016/j.scitotenv.2016.12.052, 2017.

599 Ding, A. J., Fu, C. B., Yang, X. Q., Sun, J. N., Zheng, L. F., Xie, Y. N., Herrmann, E., Nie, W., Petäjä, T., Kerminen,
600 V. M., and Kulmala, M.: Ozone and fine particle in the western Yangtze River Delta: an overview of 1 yr data at
601 the SORPES station, Atmos. Chem. Phys., 13, 5813-5830, 10.5194/acp-13-5813-2013, 2013.

602 Elshorbany, Y. F., Kurtenbach, R., Wiesen, P., Lissi, E., Rubio, M., Villena, G., Gramsch, E., Rickard, A. R., Pilling,
603 M. J., and Kleffmann, J.: Oxidation capacity of the city air of Santiago, Chile, Atmos. Chem. Phys., 9, 2257-2273,
604 10.5194/acp-9-2257-2009, 2009.

605 Elshorbany, Y. F., Kleffmann, J., Kurtenbach, R., Lissi, E., Rubio, M., Villena, G., Gramsch, E., Rickard, A. R.,
606 Pilling, M. J., and Wiesen, P.: Seasonal dependence of the oxidation capacity of the city of Santiago de Chile,
607 Atmos. Environ., 44, 5383-5394, 10.1016/j.atmosenv.2009.08.036, 2010.

608 Elshorbany, Y. F., Steil, B., Brühl, C., and Lelieveld, J.: Impact of HONO on global atmospheric chemistry
609 calculated with an empirical parameterization in the EMAC model, Atmos. Chem. Phys., 12, 9977-10000,
610 10.5194/acp-12-9977-2012, 2012.

611 Emmerson, K. M., Carslaw, N., Carslaw, D. C., Lee, J. D., McFiggans, G., Bloss, W. J., Gravestock, T., Heard, D.
612 E., Hopkins, J., Ingham, T., Pilling, M. J., Smith, S. C., Jacob, M., and Monks, P. S.: Free radical modelling studies
613 during the UK TORCH Campaign in Summer 2003, Atmos. Chem. Phys., 7, 167–181, doi:10.5194/acp-7-167-
614 2007, 2007.

615 Finlayson-Pitts, B. J., and Pitts, J. N.: Chemistry of the upper and lower atmosphere : theory, experiments and
616 applications, Academic Press, San Diego, Calif., xxii, 969 pp., 1999.

617 Finlayson-Pitts, B. J., Wingen, L. M., Sumner, A. L., Syomin, D., and Ramazan, K. A.: The heterogeneous
618 hydrolysis of NO_2 in laboratory systems and in outdoor and indoor atmospheres: An integrated mechanism, PCCP,
619 5, 223-242, 10.1039/b208564j, 2003.

620 Gall, E. T., Griffin, R. J., Steiner, A. L., Dibb, J., Scheuer, E., Gong, L., Rutter, A. P., Cevik, B. K., Kim, S., Lefer,
621 B., and Flynn, J.: Evaluation of nitrous acid sources and sinks in urban outflow, Atmos. Environ., 127, 272-282,
622 10.1016/j.atmosenv.2015.12.044, 2016.

623 George, C., Strekowski, R. S., Kleffmann, J., Stemmler, K., and Ammann, M.: Photoenhanced uptake of gaseous
624 NO_2 on solid organic compounds: a photochemical source of HONO?, Faraday Discuss., 130, 195-210,
625 10.1039/B417888M, 2005.

626 Gerecke, A., Thielmann, A., Gutzwiller, L., and Rossi, M. J.: The chemical kinetics of HONO formation resulting
627 from heterogeneous interaction of NO_2 with flame soot, Geophys. Res. Letts., 25, 2453-2456, 10.1029/98GL01796,
628 1998.

629 Gherman, T., Venables, D. S., Vaughan, S., Orphal, J., and Ruth, A. A.: Incoherent Broadband Cavity-Enhanced
630 Absorption Spectroscopy in the near-Ultraviolet: Application to HONO and NO_2, Environ. Sci. Technol., 42, 890-
631 895, 10.1021/es0716913, 2008.

632 Guo, J., Tilgner, A., Yeung, C., Wang, Z., Louie, P. K. K., Luk, C. W. Y., Xu, Z., Yuan, C., Gao, Y., Poon, S.,
633 Herrmann, H., Lee, S., Lam, K. S., and Wang, T.: Atmospheric Peroxides in a Polluted Subtropical Environment:
634 Seasonal Variation, Sources and Sinks, and Importance of Heterogeneous Processes, Environ. Sci. Technol., 48,
635 1443-1450, 10.1021/es403229x, 2014.

636 Gutzwiller, L., Arens, F., Baltensperger, U., Gäggeler, H. W., and Ammann, M.: Significance of Semivolatile Diesel
637 Exhaust Organics for Secondary HONO Formation, Environ. Sci. Technol., 36, 677-682, 10.1021/es015673b, 2002.

638 Han, C., Liu, Y., and He, H.: Heterogeneous reaction of NO_2 with soot at different relative humidity., Environ. Sci.
639 Pollut. Res., 24, 21248–21255, 10.1007/s11356-017-9766-y, 2017a.

640 Han, C., Yang, W., Yang, H., and Xue, X.: Enhanced photochemical conversion of NO_2 to HONO on humic acids
641 in the presence of benzophenone, Environ. Pollut., 231, 979-986, https://doi.org/10.1016/j.envpol.2017.08.107,
642 2017b.

643 Heard, D. E., Carpenter, L. J., Creasey, D. J., Hopkins, J. R., Lee, J. D., Lewis, A. C., Pilling, M. J., Seakins, P. W.,
644 Carslaw, N., and Emmerson, K. M.: High levels of the hydroxyl radical in the winter urban troposphere, Geophys.
645 Res. Letts., 31, 10.1029/2004gl020544, 2004.

646 Heland, J., Kleffmann, J., Kurtenbach, R., and Wiesen, P.: A New Instrument To Measure Gaseous Nitrous Acid
647 (HONO) in the Atmosphere, Environ. Sci. Technol., 35, 3207-3212, 10.1021/es000303t, 2001.

Hendrick, F., Müller, J. F., Clémer, K., Wang, P., De Mazière, M., Fayt, C., Gielen, C., Hermans, C., Ma, J. Z., Pinardi, G., Stavrakou, T., Vlemmix, T., and Van Roozendael, M.: Four years of ground-based MAX-DOAS observations of HONO and NO_2 in the Beijing area, Atmos. Chem. Phys., 14, 765-781, 10.5194/acp-14-765-2014, 2014.

Hofzumahaus, A., Rohrer, F., Lu, K., Bohn, B., Brauers, T., Chang, C. C., Fuchs, H., Holland, F., Kita, K., Kondo, Y., Li, X., Lou, S., Shao, M., Zeng, L., Wahner, A., and Zhang, Y.: Amplified trace gas removal in the troposphere, Science, 324, 1702-1704, 10.1126/science.1164566, 2009.

Hua, W., Chen, Z. M., Jie, C. Y., Kondo, Y., Hofzumahaus, A., Takegawa, N., Chang, C. C., Lu, K. D., Miyazaki, Y., Kita, K., Wang, H. L., Zhang, Y. H., and Hu, M.: Atmospheric hydrogen peroxide and organic hydroperoxides during PRIDE-PRD'06, China: their concentration, formation mechanism and contribution to secondary aerosols, Atmos. Chem. Phys., 8, 6755-6773, 10.5194/acp-8-6755-2008, 2008.

Huang, G., Zhou, X., Deng, G., Qiao, H., and Civerolo, K.: Measurements of atmospheric nitrous acid and nitric acid, Atmos. Environ., 36, 2225-2235, https://doi.org/10.1016/S1352-2310(02)00170-X, 2002.

Huang, R.-J., Yang, L., Cao, J., Wang, Q., Tie, X., Ho, K.-F., Shen, Z., Zhang, R., Li, G., Zhu, C., Zhang, N., Dai, W., Zhou, J., Liu, S., Chen, Y., Chen, J., and O'Dowd, C. D.: Concentration and sources of atmospheric nitrous acid (HONO) at an urban site in Western China, Sci. Total Environ., 593-594, 165-172, https://doi.org/10.1016/j.scitotenv.2017.02.166, 2017.

Jenkin, M. E., Saunders, S. M., and Pilling, M. J.: The tropospheric degradation of volatile organic compounds: a protocol for mechanism development, Atmos. Environ., 31, 81-104, http://dx.doi.org/10.1016/S1352-2310(96)00105-7, 1997.

Jenkin, M. E., Wyche, K. P., Evans, C. J., Carr, T., Monks, P. S., Alfarra, M. R., Barley, M. H., McFiggans, G. B., Young, J. C., and Rickard, A. R.: Development and chamber evaluation of the MCM v3.2 degradation scheme for β-caryophyllene, Atmos. Chem. Phys., 12, 5275-5308, 10.5194/acp-12-5275-2012, 2012.

Kirchstetter, T. W., Harley, A. R., and Littlejohn, D.: Measurement of nitrous acid in motor vehicle exhaust, Environ. Sci. Technol., 30, 2843–2849, 10.1021/es960135y, 1996.

Kleffmann, J., Becker, K. H., and Wiesen, P.: Heterogeneous NO2 conversion processes on acid surfaces: possible atmospheric implications, Atmos. Environ., 32, 2721-2729, https://doi.org/10.1016/S1352-2310(98)00065-X, 1998.

Kleffmann, J., Kurtenbach, R., Lörzer, J., Wiesen, P., Kalthoff, N., Vogel, B., and Vogel, H.: Measured and simulated vertical profiles of nitrous acid-Part I: Field measurements, Atmos. Environ., 37, 2949-2955, 10.1016/s1352-2310(03)00242-5, 2003.

Kleffmann, J., Gavriloaiei, T., Hofzumahaus, A., Holland, F., Koppmann, R., Rupp, L., Schlosser, E., Siese, M., and Wahner, A.: Daytime formation of nitrous acid: A major source of OH radicals in a forest, Geophys. Res. Letts., 32, L05818, 10.1029/2005GL022524, 2005.

Kleffmann, J., Lörzer, J. C., Wiesen, P., Kern, C., Trick, S., Volkamer, R., Rodenas, M., and Wirtz, K.: Intercomparison of the DOAS and LOPAP techniques for the detection of nitrous acid (HONO), Atmos. Environ., 40, 3640-3652, https://doi.org/10.1016/j.atmosenv.2006.03.027, 2006.

Kleffmann, J., and Wiesen, P.: Technical Note: Quantification of interferences of wet chemical HONO LOPAP measurements under simulated polar conditions, Atmos. Chem. Phys., 8, 6813-6822, https://doi.org/10.5194/acp-8-6813-2008, 2008.

Kurtenbach, R., Becker, K. H., Gomes, J. A. G., Kleffmann, J., Lörzer, J. C., Spittler, M., Wiesen, P., Ackermann, R., Geyer, A., and Platt, U.: Investigations of emissions and heterogeneous formation of HONO in a road traffic tunnel, Atmos. Environ., 35, 3385-3394, https://doi.org/10.1016/S1352-2310(01)00138-8, 2001.

Lee, J. D., Whalley, L. K., Heard, D. E., Stone, D., Dunmore, R. E., Hamilton, J. F., Young, D. E., Allan, J. D., Laufs, S., and Kleffmann, J.: Detailed budget analysis of HONO in central London reveals a missing daytime source, Atmos. Chem. Phys., 16, 2747-2764, 10.5194/acp-16-2747-2016, 2016.

Li, G., Lei, W., Zavala, M., Volkamer, R., Dusanter, S., Stevens, P., and Molina, L. T.: Impacts of HONO sources on the photochemistry in Mexico City during the MCMA-2006/MILAGO Campaign, Atmos. Chem. Phys., 10, 6551-6567, 10.5194/acp-10-6551-2010, 2010.

Li, X., Brauers, T., Haseler, R., Bohn, B., Fuchs, H., Hofzumahaus, A., Holland, F., Lou, S., Lu, K. D., Rohrer, F., Hu, M., Zeng, L. M., Zhang, Y. H., Garland, R. M., Su, H., Nowak, A., Wiedensohler, A., Takegawa, N., Shao, M., and Wahner, A.: Exploring the atmospheric chemistry of nitrous acid (HONO) at a rural site in Southern China, Atmos. Chem. Phys., 12, 1497-1513, 10.5194/acp-12-1497-2012, 2012.

Liang, Y., Zha, Q., Wang, W., Cui, L., Lui, K. H., Ho, K. F., Wang, Z., Lee, S.-c., and Wang, T.: Revisiting nitrous acid (HONO) emission from on-road vehicles: A tunnel study with a mixed fleet, J. Air Waste Manage., 67, 797-805, 10.1080/10962247.2017.1293573, 2017.

Lu, K. D., Rohrer, F., Holland, F., Fuchs, H., Bohn, B., Brauers, T., Chang, C. C., Häseler, R., Hu, M., Kita, K., Kondo, Y., Li, X., Lou, S. R., Nehr, S., Shao, M., Zeng, L. M., Wahner, A., Zhang, Y. H., and Hofzumahaus, A.: Observation and modelling of OH and HO2 concentrations in the Pearl River Delta 2006: a missing OH source in a VOC rich atmosphere, Atmos. Chem. Phys., 12, 1541-1569, 10.5194/acp-12-1541-2012, 2012.

Ma, Y., Diao, Y., Zhang, B., Wang, W., Ren, X., Yang, D., Wang, M., Shi, X., and Zheng, J.: Detection of formaldehyde emissions from an industrial zone in the Yangtze River Delta region of China using a proton transfer reaction ion-drift chemical ionization mass spectrometer, Atmos. Meas. Tech., 9, 6101-6116, 10.5194/amt-9-6101-2016, 2016.

Makkonen, U., Virkkula, A., Mäntykenttä, J., Hakola, H., Keronen, P., Vakkari, V., and Aalto, P. P.: Semi-continuous gas and inorganic aerosol measurements at a Finnish urban site: comparisons with filters, nitrogen in aerosol and gas phases, and aerosol acidity, Atmospheric Chemistry and Physics, 12, 5617-5631, 10.5194/acp-12-5617-2012, 2012.

Michoud, V., Colomb, A., Borbon, A., Miet, K., Beekmann, M., Camredon, M., Aumont, B., Perrier, S., Zapf, P., Siour, G., Ait-Helal, W., Afif, C., Kukui, A., Furger, M., Dupont, J. C., Haeffelin, M., and Doussin, J. F.: Study of the unknown HONO daytime source at a European suburban site during the MEGAPOLI summer and winter field campaigns, Atmospheric Chemistry and Physics, 14, 2805-2822, 10.5194/acp-14-2805-2014, 2014.

Monge, M. E., D'Anna, B., Mazri, L., Giroir-Fendler, A., Ammann, M., Donaldson, D. J., and George, C.: Light changes the atmospheric reactivity of soot, Proc. Natl. Acad. Sci. USA, 107, 6605-6609, 10.1073/pnas.0908341107, 2010.

Müller, M., Anderson, B. E., Beyersdorf, A. J., Crawford, J. H., Diskin, G. S., Eichler, P., Fried, A., Keutsch, F. N., Mikoviny, T., Thornhill, K. L., Walega, J. G., Weinheimer, A. J., Yang, M., Yokelson, R. J., and Wisthaler, A.: In situ measurements and modeling of reactive trace gases in a small biomass burning plume, Atmos. Chem. Phys., 16, 3813-3824, 10.5194/acp-16-3813-2016, 2016.

Nakashima, Y., and Kajii, Y.: Determination of nitrous acid emission factors from a gasoline vehicle using a chassis dynamometer combined with incoherent broadband cavity-enhanced absorption spectroscopy, Sci. Total Environ., 575, 287-293, https://doi.org/10.1016/j.scitotenv.2016.10.050, 2017.

Nash, T.: Nitrous acid in the atmosphere and laboratory experiments on its photolysis, Tellus, 26, 175-179, 10.3402/tellusa.v26i1-2.9768, 1974.

Ndour, M., D'Anna, B., George, C., Ka, O., Balkanski, Y., Kleffmann, J., Stemmler, K., and Ammann, M.: Photoenhanced uptake of NO_2 on mineral dust: Laboratory experiments and model simulations, Geophys. Res. Letts., 35, L05812, 10.1029/2007gl032006, 2008.

Neftel, A., Blatter, A., Hesterberg, R., and Staffelbach, T.: Measurements of concentration gradients of HNO_2 and HNO_3 over a semi-natural ecosystem Atmos. Environ., 30 (17), 3017-3025, 1996.

Neuman, J. A., Trainer, M., Brown, S. S., Min, K.-E., Nowak, J. B., Parrish, D. D., Peischl, J., Pollack, I. B., Roberts, J. M., Ryerson, T. B., and Veres, P. R.: HONO emission and production determined from airborne measurements over the Southeast U.S., J. Geophys. Res. Atmos., 121, 9237–9250, 10.1002/2016JD025197, 2016.

Nie, W., Ding, A. J., Xie, Y. N., Xu, Z., Mao, H., Kerminen, V. M., Zheng, L. F., Qi, X. M., Huang, X., Yang, X. Q., Sun, J. N., Herrmann, E., Petaja, T., Kulmala, M., and Fu, C. B.: Influence of biomass burning plumes on HONO chemistry in eastern China, Atmos. Chem. Phys., 15, 1147-1159, 10.5194/acp-15-1147-2015, 2015.

Perner, D., and Platt, U.: Detection of nitrous-acid in the atmosphere by differential optical-absorption, Geophys. Res. Letts., 6, 917-920, 10.1029/GL006i012p00917, 1979.

Pinto, J. P., Dibb, J., Lee, B. H., Rappenglück, B., Wood, E. C., Levy, M., Zhang, R. Y., Lefer, B., Ren, X. R., Stutz, J., Tsai, C., Ackermann, L., Golovko, J., Herndon, S. C., Oakes, M., Meng, Q. Y., Munger, J. W., Zahniser, M., and Zheng, J.: Intercomparison of field measurements of nitrous acid (HONO) during the SHARP campaign, J. Geophys. Res. Atmos., 119, 5583-5601, 10.1002/2013JD020287, 2014.

Platt, U., Perner, D., Harris, G. W., Winer, A. M., and Pitts Jr, J. N.: Observations of nitrous acid in an urban atmosphere by differential optical absorption, Nature, 285, 312, 10.1038/285312a0, 1980.

Qin, M., Xie, P., Su, H., Gu, J., Peng, F., Li, S., Zeng, L., Liu, J., Liu, W., and Zhang, Y.: An observational study of the HONO-NO_2 coupling at an urban site in Guangzhou City, South China, Atmos. Environ., 43, 5731-5742, https://doi.org/10.1016/j.atmosenv.2009.08.017, 2009.

Rairoux, P., Koch, B., Moller, D., Göritz, G., Warmbier, G., and Czyzewski, A.: Atmospheric traces monitoring applying Cavity Ring-Down Spectroscopy, Environ. Sci. Pollut. Res., Special issue 4, 68-71, 2002.

Ren, X., Brune, W. H., Mao, J., Mitchell, M. J., Lesher, R. L., Simpas, J. B., Metcalf, A. R., Schwab, J. J., Li, Y., Demerjian, K. L., Felton, H. D., Boynton, G., Adams, A., Perry, J., He, Y., Zhou, X., and Hou, J.: Behavior of OH and HO2 in the winter atmosphere in New York City: Observations and model comparison, Atmos. Environ., 40, S252–S263, 10.1016/j.atmosenv.2005.11.073, 2006.

760 Ren, X., Gao, H., Zhou, X., Crounse, J. D., Wennberg, P. O., Browne, E. C., LaFranchi, B. W., Cohen, R. C., McKay,
761 M., Goldstein, A. H., and Mao, J.: Measurement of atmospheric nitrous acid at Blodgett Forest during
762 BEARPEX2007, Atmos. Chem. Phys., 10, 6283-6294, 10.5194/acp-10-6283-2010, 2010.

763 Ren, X. R., Harder, H., Martinez, M., Lesher, R. L., Oliger, A., Simpas, J. B., Brune, W. H., Schwab, J. J., Demerjian,
764 K. L., He, Y., Zhou, X. L., and Gao, H. G.: OH and HO2 chemistry in the urban atmosphere of New York City,
765 Atmos. Environ., 37, 3639-3651, 10.1016/s1352-2310(03)00459-x, 2003.

766 Ren, Y., Ding, A., Wang, T., Shen, X., Guo, J., Zhang, J., Wang, Y., Xu, P., Wang, X., and Gao, J.: Measurement of
767 gas-phase total peroxides at the summit of Mount Tai in China, Atmospheric Environment, 43, 1702-1711,
768 10.1016/j.atmosenv.2008.12.020, 2009.

769 Rickard, A. R., Johnson, D., McGill, C. D., and Marston, G.: OH Yields in the Gas-Phase Reactions of Ozone with
770 Alkenes, The Journal of Physical Chemistry A, 103, 7656-7664, 10.1021/jp9916992, 1999.

771 Rondon, A., and Sanhueza, E.: High HONO atmospheric concentrations during vegetation burning in the tropical
772 savannah, Tellus B: Chem. Phys. Meteor., 41, 474-477, 10.3402/tellusb.v41i4.15102, 1989.

773 Salmon, O. E., Shepson, P. B., Ren, X., He, H., Hall, D. L., Dickerson, R. R., Stirm, B. H., Brown, S. S., Fibiger,
774 D. L., McDuffie, E. E., Campos, T. L., Gurney, K. R., and Thornton, J. A.: Top-Down Estimates of NO_x and CO
775 Emissions From Washington, D.C.-Baltimore During the WINTER Campaign, J. Geophys. Res. Atmos., 123,
776 7705–7724, 10.1029/2018jd028539, 2018.

777 Scharko, N. K., Martin, E. T., Losovyj, Y., Peters, D. G., and Raff, J. D.: Evidence for Quinone Redox Chemistry
778 Mediating Daytime and Nighttime NO_2-to-HONO Conversion on Soil Surfaces, Environ. Sci. Technol., 51, 9633-
779 9643, 10.1021/acs.est.7b01363, 2017.

780 Sörgel, M., Trebs, I., Wu, D., and Held, A.: A comparison of measured HONO uptake and release with calculated
781 source strengths in a heterogeneous forest environment, Atmospheric Chemistry and Physics, 15, 9237-9251,
782 10.5194/acp-15-9237-2015, 2015.

783 Spataro, F., Ianniello, A., Esposito, G., Allegrini, I., Zhu, T., and Hu, M.: Occurrence of atmospheric nitrous acid
784 in the urban area of Beijing (China), Sci. Total Environ., 447, 210-224,
785 https://doi.org/10.1016/j.scitotenv.2012.12.065, 2013.

786 Stemmler, K., Ammann, M., Donders, C., Kleffmann, J., and George, C.: Photosensitized reduction of nitrogen
787 dioxide on humic acid as a source of nitrous acid, Nature, 440, 195-198, 10.1038/nature04603, 2006.

788 Stemmler, K., Ndour, M., Elshorbany, Y., Kleffmann, J., D'Anna, B., George, C., Bohn, B., and Ammann, M.: Light
789 induced conversion of nitrogen dioxide into nitrous acid on submicron humic acid aerosol, Atmos. Chem. Phys., 7,
790 4237-4248, 10.5194/acp-7-4237-2007, 2007.

791 Stutz, J., Alicke, B., Ackermann, R., Geyer, A., Wang, S. H., White, A. B., Williams, E. J., Spicer, C. W., and Fast,
792 J. D.: Relative humidity dependence of HONO chemistry in urban areas, J. Geophys. Res. Atmos., 109, D03307,
793 doi:10.1029/2003jd004135, 2004.

794 Su, H., Cheng, Y. F., Shao, M., Gao, D. F., Yu, Z. Y., Zeng, L. M., Slanina, J., Zhang, Y. H., and Wiedensohler, A.:
795 Nitrous acid (HONO) and its daytime sources at a rural site during the 2004 PRIDE-PRD experiment in China, J.
796 Geophys. Res. Atmos., 113, D14312, 10.1029/2007JD009060, 2008.

Su, H., Cheng, Y., Oswald, R., Behrendt, T., Trebs, I., Meixner, F. X., Andreae, M. O., Cheng, P., Zhang, Y., and Poschl, U.: Soil nitrite as a source of atmospheric HONO and OH radicals, Science, 333, 1616-1618, 10.1126/science.1207687, 2011.

Tang, Y., An, J., Wang, F., Li, Y., Qu, Y., Chen, Y., and Lin, J.: Impacts of an unknown daytime HONO source on the mixing ratio and budget of HONO, and hydroxyl, hydroperoxyl, and organic peroxy radicals, in the coastal regions of China, Atmos. Chem. Phys., 15, 9381-9398, 10.5194/acp-15-9381-2015, 2015.

Tanner, D. J., and Eisele, F. L.: Present oh measurement limits and associated uncertainties, J. Geophys. Res. Atmos., 100, 2883-2892, 1995.

Trick, S.: Formation of nitrous acid on urban surfaces - a physicalchemical perspective, Ph.D. thesis, University of Heidelberg, 2004.

Trinh, H. T., Imanishi, K., Morikawa, T., Hagino, H., and Takenaka, N.: Gaseous nitrous acid (HONO) and nitrogen oxides (NO_x) emission from gasoline and diesel vehicles under real-world driving test cycles, J. Air Waste Manage., 67, 412-420, 10.1080/10962247.2016.1240726, 2017.

VandenBoer, T. C., Brown, S. S., Murphy, J. G., Keene, W. C., Young, C. J., Pszenny, A. A. P., Kim, S., Warneke, C., de Gouw, J. A., Maben, J. R., Wagner, N. L., Riedel, T. P., Thornton, J. A., Wolfe, D. E., Dubé, W. P., Öztürk, F., Brock, C. A., Grossberg, N., Lefer, B., Lerner, B., Middlebrook, A. M., and Roberts, J. M.: Understanding the role of the ground surface in HONO vertical structure: High resolution vertical profiles during NACHTT-11, J. Geophys. Res. Atmos., 118, 10,155-110,171, 10.1002/jgrd.50721, 2013.

Vecera, Z., and Dasgupta, P. K.: Measurement of ambient nitrous acid and a reliable calibration source for gaseous nitrous acid, Environ. Sci. Technol., 25, 255-260, 10.1021/es00014a006, 1991.

Villena, G., Kleffmann, J., Kurtenbach, R., Wiesen, P., Lissi, E., Rubio, M. A., Croxatto, G., and Rappenglück, B.: Vertical gradients of HONO, NOx and O3 in Santiago de Chile, Atmos. Environ., 45, 3867-3873, 10.1016/j.atmosenv.2011.01.073, 2011.

Villena, G., Bejan, I., Kurtenbach, R., Wiesen, P., and Kleffmann, J.: Interferences of commercial NO_2 instruments in the urban atmosphere and in a smog chamber, Atmos. Meas. Tech., 5, 149-159, 10.5194/amt-5-149-2012, 2012.

Wall, K. J., and Harris, G. W.: Uptake of nitrogen dioxide (NO_2) on acidic aqueous humic acid (HA) solutions as a missing daytime nitrous acid (HONO) surface source, J. Atmos. Chem., 74, 283-321, 10.1007/s10874-016-9342-8, 2016.

Wang, J., Zhang, X., Guo, J., Wang, Z., and Zhang, M.: Observation of nitrous acid (HONO) in Beijing, China: Seasonal variation, nocturnal formation and daytime budget, Sci. Total Environ., 587-588, 350-359, https://doi.org/10.1016/j.scitotenv.2017.02.159, 2017.

Wang, L., Wen, L., Xu, C., Chen, J., Wang, X., Yang, L., Wang, W., Yang, X., Sui, X., Yao, L., and Zhang, Q.: HONO and its potential source particulate nitrite at an urban site in North China during the cold season, The Science of the total environment, 538, 93-101, 10.1016/j.scitotenv.2015.08.032, 2015a.

Wang, M., Chen, W. T., Shao, M., Lu, S. H., Zeng, L. M., and Hu, M.: Investigation of carbonyl compound sources at a rural site in the Yangtze River Delta region of China, Journal of Environmental Sciences-China, 28, 128-136, 10.1016/j.jes.2014.12.001, 2015b.

Wang, S., Zhou, R., Zhao, H., Wang, Z., Chen, L., and Zhou, B.: Long-term observation of atmospheric nitrous acid (HONO) and its implication to local NO_2 levels in Shanghai, China, Atmos. Environ., 77, 718-724, https://doi.org/10.1016/j.atmosenv.2013.05.071, 2013.

Wong, K. W., Oh, H. J., Lefer, B. L., Rappenglück, B., and Stutz, J.: Vertical profiles of nitrous acid in the nocturnal urban atmosphere of Houston, TX, Atmos. Chem. Phys., 11, 3595-3609, 10.5194/acp-11-3595-2011, 2011.

Wong, K. W., Tsai, C., Lefer, B., Haman, C., Grossberg, N., Brune, W. H., Ren, X., Luke, W., and Stutz, J.: Daytime HONO vertical gradients during SHARP 2009 in Houston, TX, Atmospheric Chemistry and Physics, 12, 635-652, 10.5194/acp-12-635-2012, 2012.

Wong, K. W., Tsai, C., Lefer, B., Grossberg, N., and Stutz, J.: Modeling of daytime HONO vertical gradients during SHARP 2009, Atmos. Chem. Phys., 13, 3587-3601, 10.5194/acp-13-3587-2013, 2013.

Xu, Z., Wang, T., Wu, J., Xue, L., Chan, J., Zha, Q., Zhou, S., Louie, P. K. K., and Luk, C. W. Y.: Nitrous acid (HONO) in a polluted subtropical atmosphere: Seasonal variability, direct vehicle emissions and heterogeneous production at ground surface, Atmos. Environ., 106, 100-109, http://dx.doi.org/10.1016/j.atmosenv.2015.01.061, 2015.

Xue, L., Gu, R., Wang, T., Wang, X., Saunders, S., Blake, D., Louie, P. K. K., Luk, C. W. Y., Simpson, I., Xu, Z., Wang, Z., Gao, Y., Lee, S., Mellouki, A., and Wang, W.: Oxidative capacity and radical chemistry in the polluted atmosphere of Hong Kong and Pearl River Delta region: analysis of a severe photochemical smog episode, Atmospheric Chemistry and Physics, 16, 9891-9903, 10.5194/acp-16-9891-2016, 2016.

Ye, C., Zhou, X., Pu, D., Stutz, J., Festa, J., Spolaor, M., Tsai, C., Cantrell, C., Mauldin, R. L., Campos, T., Weinheimer, A., Hornbrook, R. S., Apel, E. C., Guenther, A., Kaser, L., Yuan, B., Karl, T., Haggerty, J., Hall, S., Ullmann, K., Smith, J. N., Ortega, J., and Knote, C.: Rapid cycling of reactive nitrogen in the marine boundary layer, Nature, 532, 489-491, 10.1038/nature17195, 2016.

Ye, C., Zhang, N., Gao, H., and Zhou, X.: Photolysis of Particulate Nitrate as a Source of HONO and NO_x, Environ. Sci. Technol., 51, 6849-6856, 10.1021/acs.est.7b00387, 2017.

Zhang, N., Zhou, X., Shepson, P. B., Gao, H., Alaghmand, M., and Stirm, B.: Aircraft measurement of HONO vertical profiles over a forested region, Geophys. Res. Letts., 36, L15820, 10.1029/2009gl038999, 2009.

Zheng, J., Ma, Y., Chen, M., Zhang, Q., Wang, L., Khalizov, A. F., Yao, L., Wang, Z., Wang, X., and Chen, L.: Measurement of atmospheric amines and ammonia using the high resolution time-of-flight chemical ionization mass spectrometry, Atmos. Environ., 102, 249-259, http://dx.doi.org/10.1016/j.atmosenv.2014.12.002, 2015a.

Zheng, J., Ma, Y., Chen, M., Zhang, Q., Wang, L., Khalizov, A. F., Yao, L., Wang, Z., Wang, X., and Chen, L.: Measurement of atmospheric amines and ammonia using the high resolution time-of-flight chemical ionization mass spectrometry, Atmospheric Environment, 102, 249-259, 10.1016/j.atmosenv.2014.12.002, 2015b.

Zhou, X., Civerolo, K., Dai, H., Huang, G., Schwab, J., and Demerjian, K.: Summertime nitrous acid chemistry in the atmospheric boundary layer at a rural site in New York State, J. Geophys. Res. Atmos., 107, ACH 13-11-ACH 13-11, 10.1029/2001jd001539, 2002.

Zhou, X., Gao, H., He, Y., Huang, G., Bertman, S. B., Civerolo, K., and Schwab, J.: Nitric acid photolysis on surfaces in low-NOxenvironments: Significant atmospheric implications, Geophys. Res. Letts., 30, 2217,

871 10.1029/2003gl018620, 2003.

872 Zhou, X., Zhang, N., TerAvest, M., Tang, D., Hou, J., Bertman, S., Alaghmand, M., Shepson, P. B., Carroll, M. A.,
873 Griffith, S., Dusanter, S., and Stevens, P. S.: Nitric acid photolysis on forest canopy surface as a source for
874 tropospheric nitrous acid, Nat. Geosci., 4, 440-443, 10.1038/ngeo1164, 2011.

875 Ziemba, L. D., Dibb, J. E., Griffin, R. J., Anderson, C. H., Whitlow, S. I., Lefer, B. L., Rappenglück, B., and Flynn,
876 J.: Heterogeneous conversion of nitric acid to nitrous acid on the surface of primary organic aerosol in an urban
877 atmosphere, Atmos. Environ., 44, 4081-4089, 10.1016/j.atmosenv.2008.12.024, 2010.

878

879

880 **Table 1.** Overview on HONO measurements performed in Nanjing and other cities in China.

Location	Date	HONO (ppbv)[#]	References
Beijing	Sep. - Oct. 2015 (autumn)	2.27 ± 1.82	Wang et al. (2017)
	Jan. 2016 (winter)	1.05 ± 0.89	
	Apr. - May 2016 (spring)	1.05 ± 0.95	
	Jun. - Jul. 2016 (summer)	1.38 ± 0.90	
Xi'an	Jul. - Aug. 2015 (summer)	1.12 ± 0.97	Huang et al. (2017)
Jinan	Nov. 2013 - Jan. 2014 (winter)	0.35 ± 0.5	Wang et al. (2015a)
Nanjing	Apr. - Jun. 2012 (spring)	0.76 ± 0.79	Nie et al. (2015)
Xianghe	Mar 2010 - Dec 2012	0.33 ± 0.16[*]	Hendrick et al. (2014)
Beijing	Jan. - Feb. 2007(winter)	1.04 ± 0.73	Spataro et al. (2013)
Guangzhou	Jul. 2006 (summer)	0.71~8.43 (2.8)[**]	Qin et al. (2009)
Xinken	Oct. - Nov. 2004 (autumn)	0.4~3.8 (1.2)[**]	Li et al. (2012)
Nanjing	Dec. 2015 (winter)	1.32 ± 0.92	This work

881 [#]Campaign averaged; [*]Yearly average; [**]Only range and mean values are reported

882

883 **Table 2.** Ozonolysis reaction rate constants and OH formation yields of the volatile organic compounds (VOC)
884 used in the calculation.

VOC	k(298K) × 10^{-18} ($cm^3molecule^{-1}s^{-1}$)[a]	OH yield	VOC	k(298K) × 10^{-18} ($cm^3molecule^{-1}s^{-1}$)[a]	OH yield
Ethene	1.6	0.13[b]	trans-2-Pentene	160	0.47[c]
Propene	10.1	0.34[b]	cis-2-Pentene	130	0.3[c]
trans-2-Butene	190	0.59[b]	1-Pentene	10.6	0.37[b]
cis-2-Butene	125	0.37[b]	Isoprene	12.8[c]	0.13 ± 0.03[c]
1-Butene	9.64	0.41[b]	Styrene	17	0.07[c]

885 a: Atkinson and Arey (2003); b: Rickard et al. (1999); c: Alicke et al. (2002)

886

887 **Table 3.** Linear correlation coefficients (Pearson correlation, R) of the unknown source to HONO production-

888 related parameters.

Individual	Correlation Coefficient (R)	Various Combinations of	Correlation Coefficient (R)
RH	0.27	$J(NO_2)\cdot S/V$	0.59
NO_2	0.31	$J(NO_2)\cdot NO_2$	0.51
S/V	0.33	$J(NO_2)\cdot RH$	0.59
$J(NO_2)$	0.31	$J(NO_2)\cdot NO_2\cdot RH$	0.70
$NO_2\cdot S/V$	0.36	$J(NO_2)\cdot NO_2\cdot S/V$	0.61
$NO_2\cdot RH$	0.40	$NO_2\cdot RH\cdot S/V$	0.44
$RH\cdot S/V$	0.39	$J(NO_2)\cdot NO_2\cdot S/V\cdot RH$	0.70

889

890

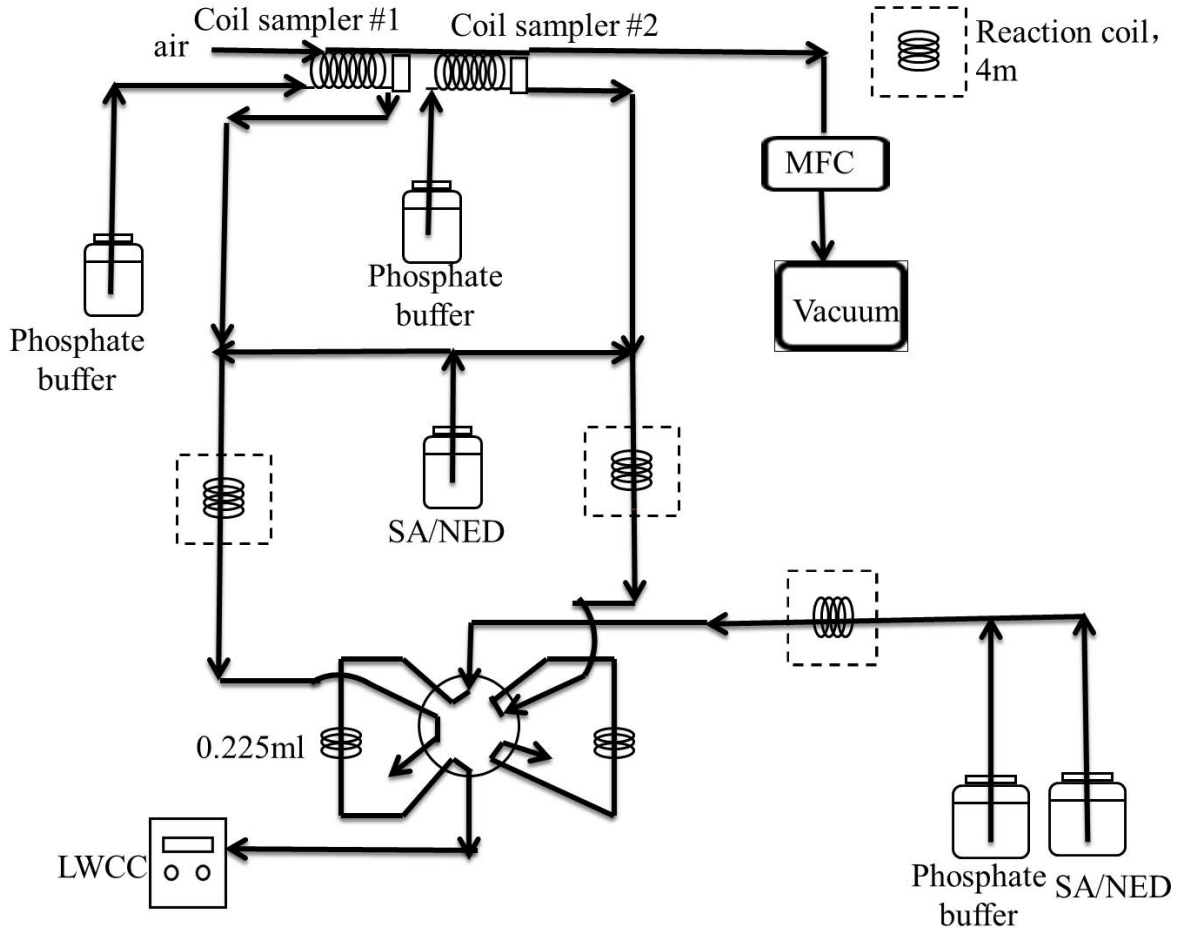

891

892 **Figure 1.** Schematics of the custom-built wet chemistry-based HONO instrument.

893

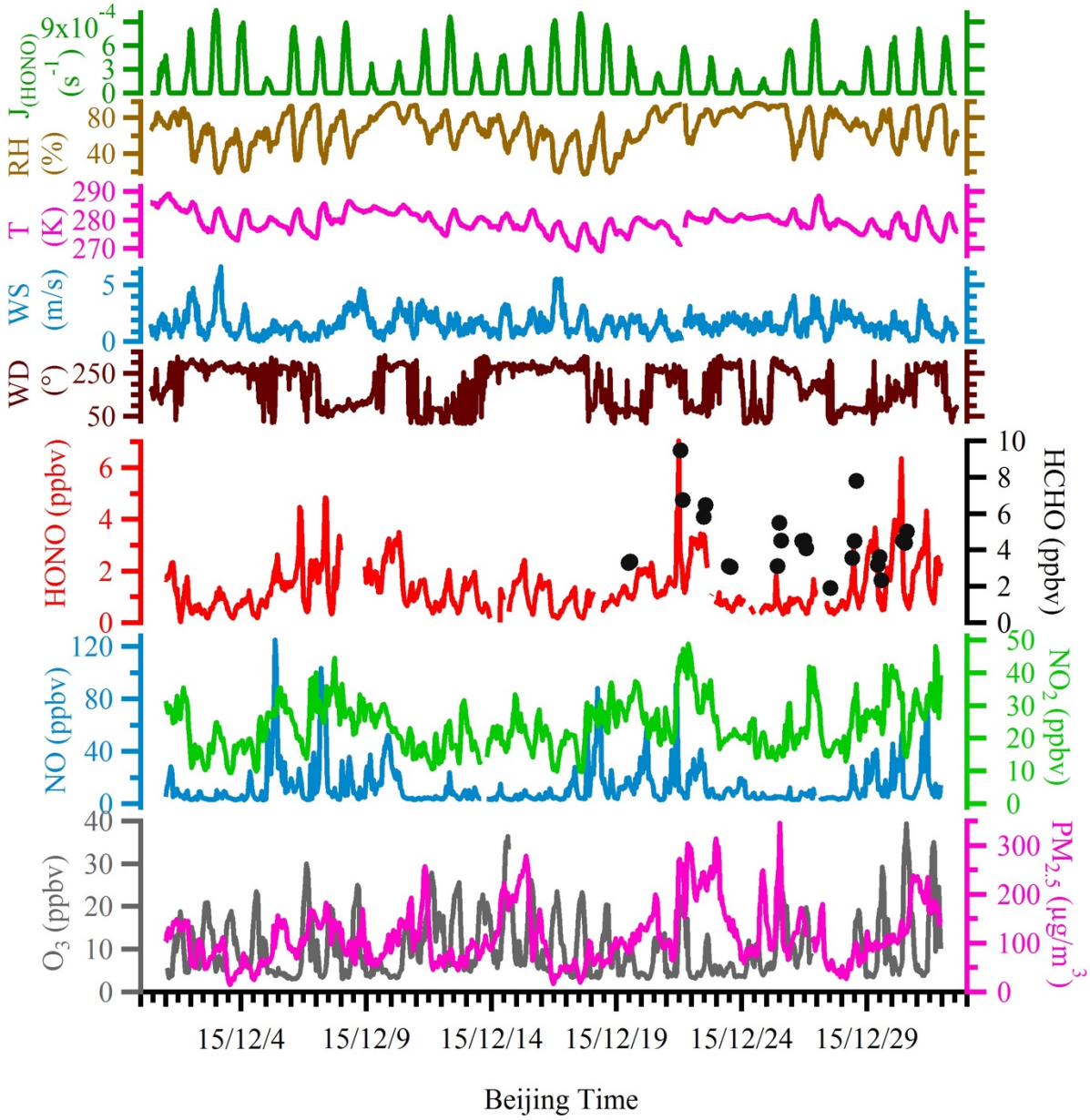

894

895 **Figure 2.** Time series of meteorological parameters, including HONO photolysis frequency (J(HONO)), relative

896 humidity (RH), ambient temperature, wind speed and wind direction, as well as mixing ratios of measured HONO,

897 HCHO, NO, NO_2, O_3 and $PM_{2.5}$ during the observation period.

898

899

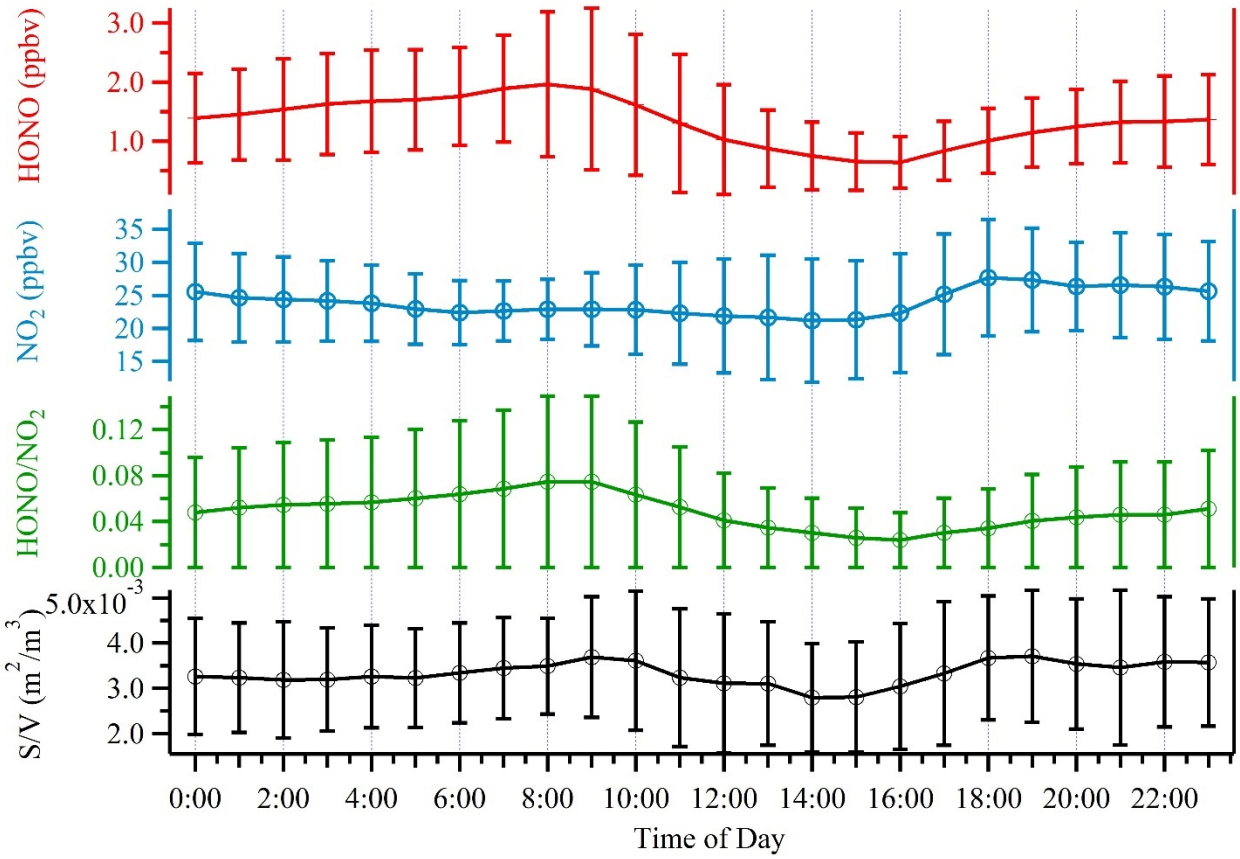

900

901 **Figure 3.** Average diurnal profiles of HONO, NO_2, HONO/NO_2 and S/V. Error bars represent the standard

902 deviations in hourly bins.

903

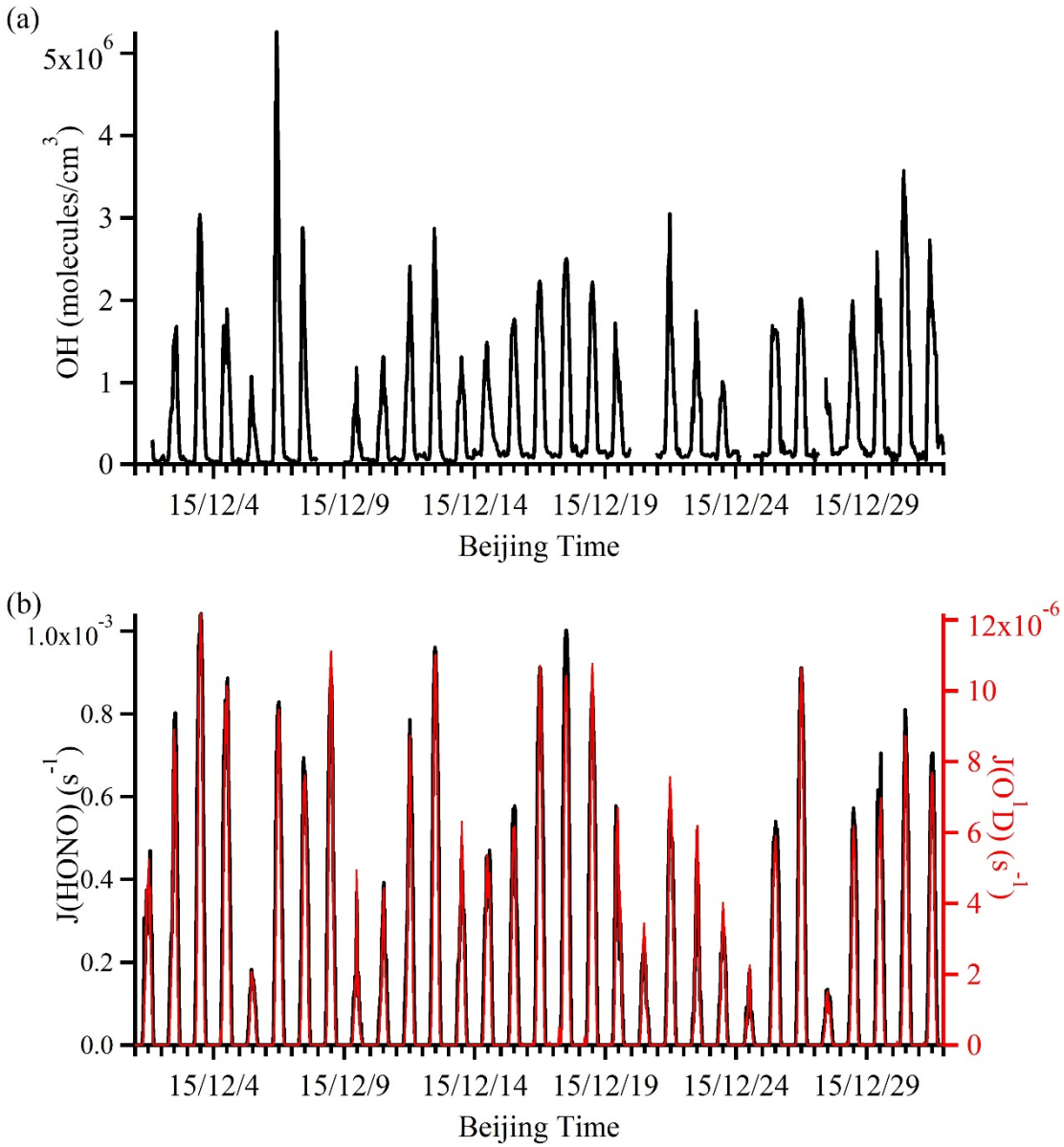

904

905

906 **Figure 4.** Time series of simulated OH (panel a) and observed photolysis rates (J(HONO) and J(O^1D)) (panel b).

907 The gaps in the OH time series were the time periods when some observation data were not available.

908

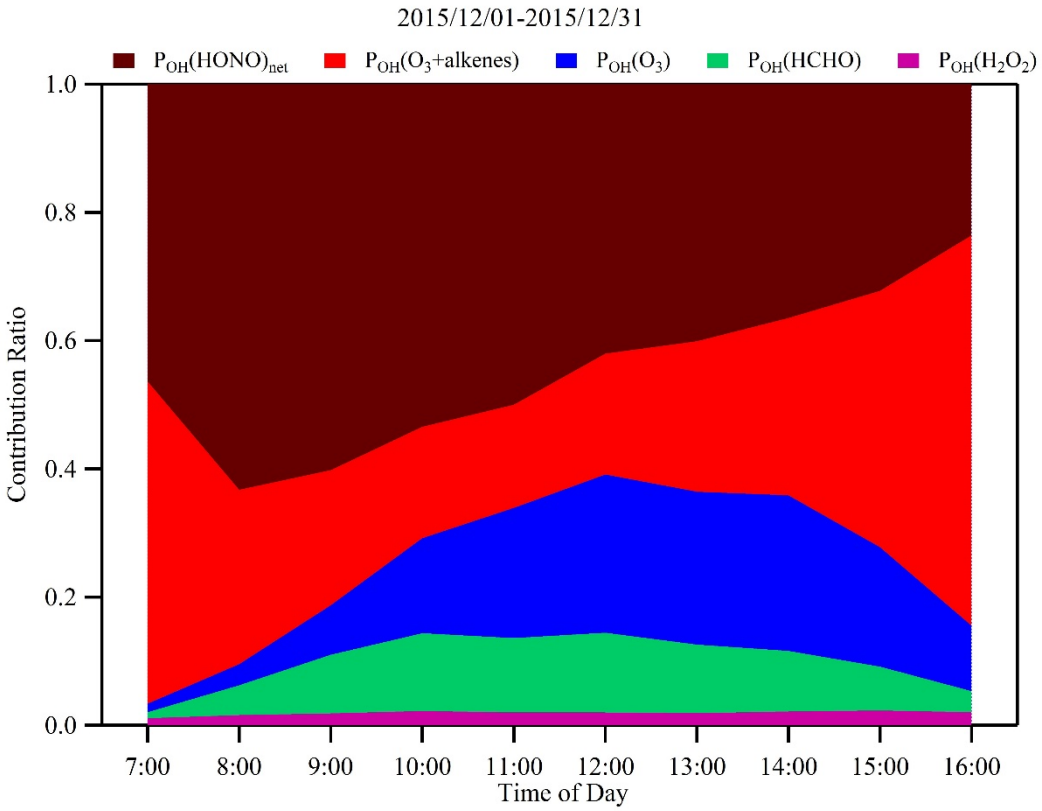

Figure 5. Campaign averaged diurnal variations of contribution fractions of OH production rates from HONO photolysis (brown), alkene ozonolysis (red), O_3 photolysis (blue), HCHO photolysis (green), and H_2O_2 photolysis (purple).

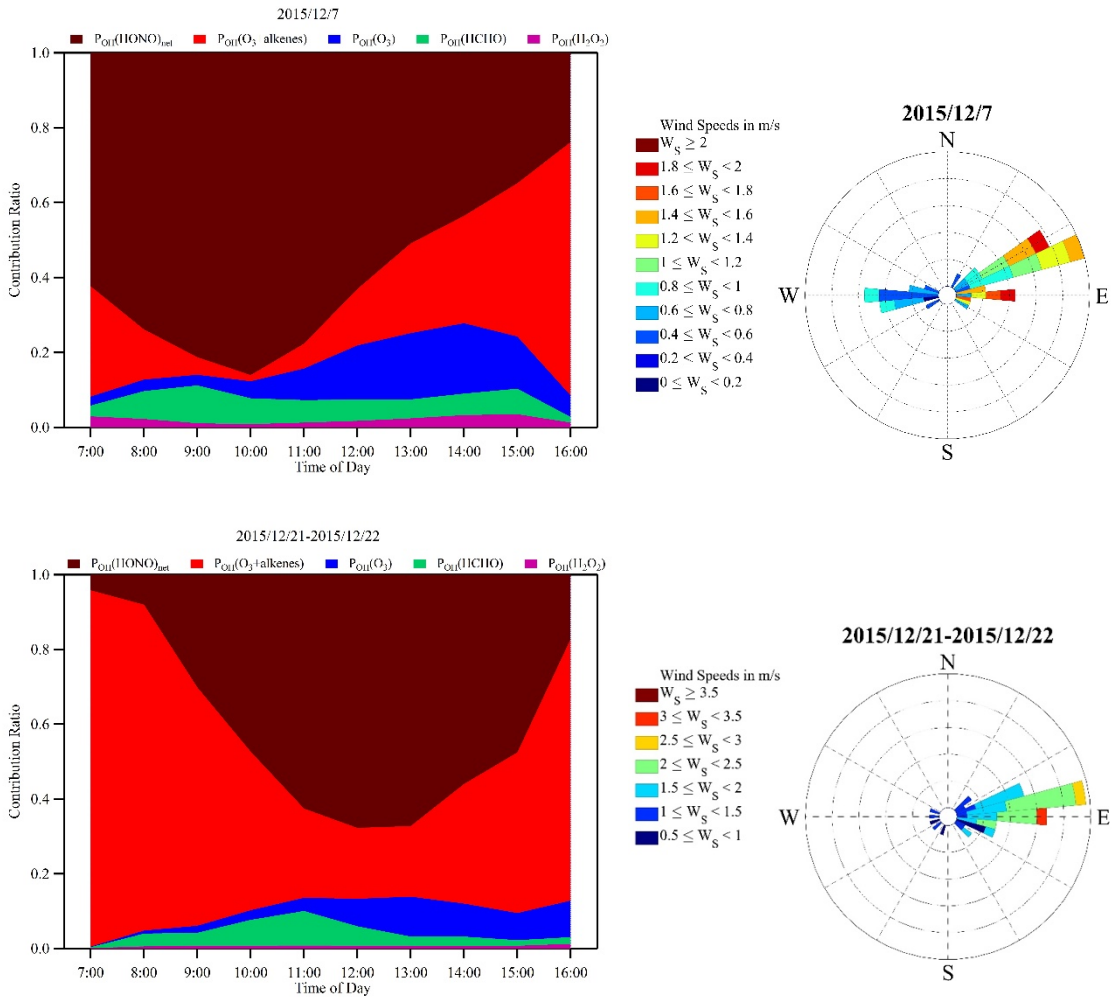

Figure 6. The same plots as Fig. 5 during two industrial plume events on the 7th (upper panel) and from the 21st-22nd (lower panel) of December 2015. The corresponding wind rose plots indicate the origin of these plumes, i.e., the industry park to the east of the observation site.

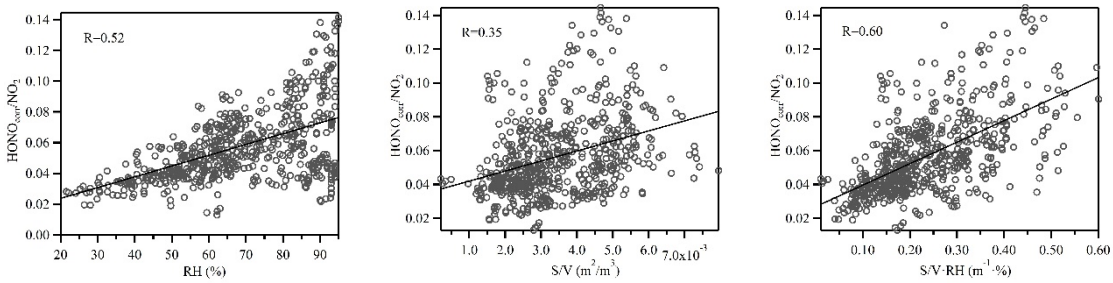

Figure 7. Nighttime correlations between $HONO/NO_2$ and RH, S/V and the product of S/V·RH.

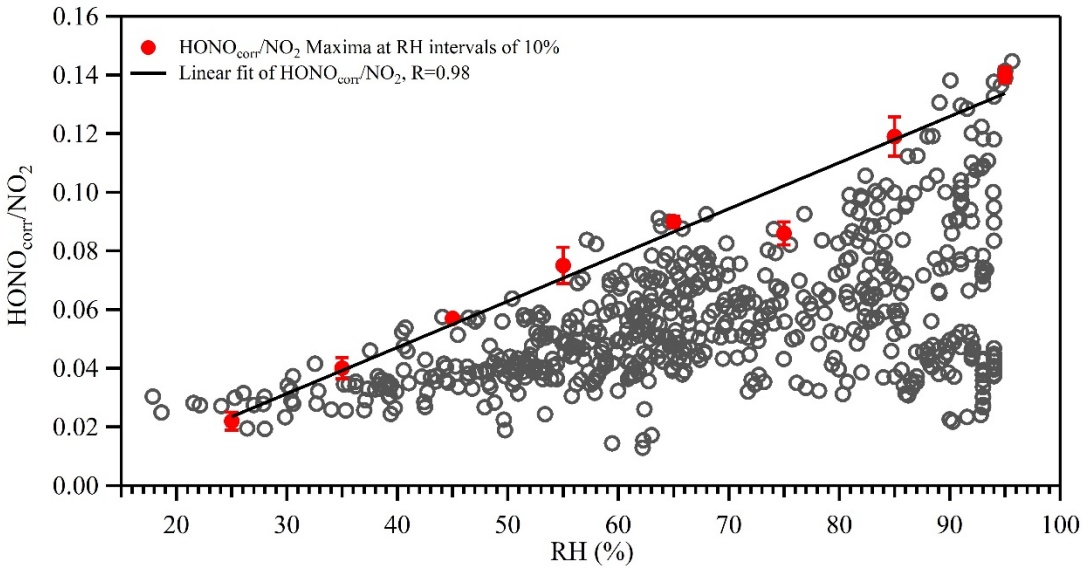

926

927 **Figure 8.** Correlation between HONO/NO_2 and relative humidity (RH) at night. The open gray circles are 30-min

928 averages. The red circles represent the averages of the top-5 maxima of HONO/NO_2 ratios in 10% RH bins. Error

929 bars represent standard deviations of the top-5 HONO/NO_2 ratios in 10% RH bins. The black line is the linear fit

930 of the red circles for HONO/NO_2 with RH.

931

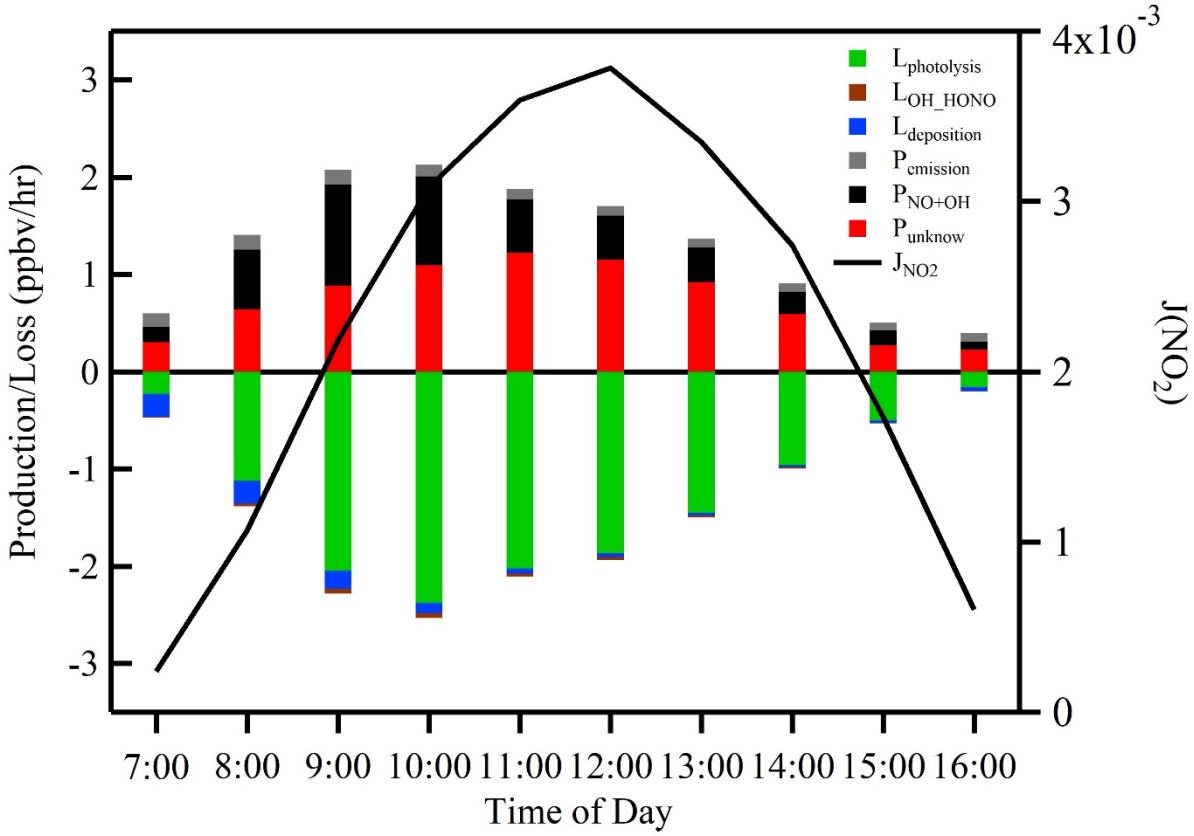

932

933 **Figure 9.** Averaged production and loss rates of daytime HONO and J(NO_2) during the measurement period. The

934 black line shows the photolysis rate of NO_2.

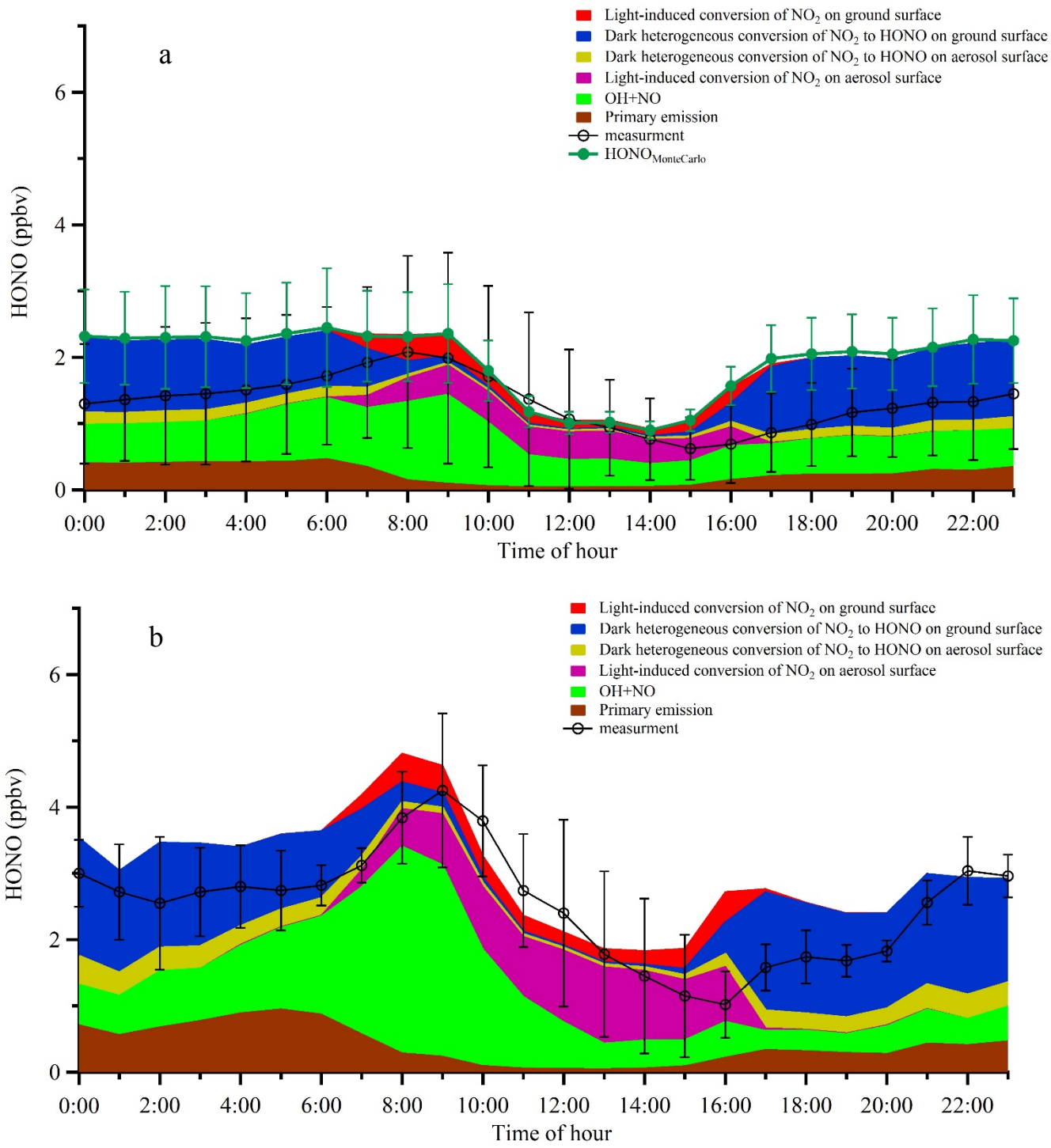

935 **Figure 10.** a) Averaged diurnal profiles of the measured HONO and the modeled HONO from different sources.

936 Error bars on the black line represent standard deviations of HONO measurements in hourly bins. Error bars on the

937 green markers denote the Monte Carlo analysis results; b) The same plot as panel a, except that only the two

938 industrial plume events (the 7th and from the 21st to 22nd of December 2015) were considered in the model.

939